Imposed currents in galvanic cells

Biesheuvel, P.M., Van Soestbergen, M., & Bazant, M.Z.

Imposed currents in galvanic cells

P.M. Biesheuvel,[1,*] M. van Soestbergen[2] and M.Z. Bazant[3]

[1]*Department of Environmental Technology, Wageningen University, Bomenweg 2, 6703 HD Wageningen, The Netherlands.* [2]*Department of Precision and Microsystems Engineering, Delft University of Technology, Mekelweg 2, 2628 CD Delft, the Netherlands.* [3]*Departments of Chemical Engineering and Mathematics, Massachusetts Institute of Technology, Cambridge ,MA 02139, USA.*

*E-mail: maarten.biesheuvel@wur.nl.

Abstract

We analyze the steady-state behavior of a general mathematical model for reversible galvanic cells, such as redox flow cells, reversible solid oxide fuel cells, and rechargeable batteries. We consider not only operation in the galvanic discharging mode, spontaneously generating a positive current against an external load, but also operation in two modes which require a net input of electrical energy: (i) the electrolytic charging mode, where a negative current is imposed to generate a voltage exceeding the open circuit voltage, and (ii) the "super-galvanic" discharging mode, where a positive current exceeding the short-circuit current is imposed to generate a negative voltage. Analysis of the various (dis-)charging modes of galvanic cells is important to predict the efficiency of electrical to chemical energy conversion and to provide sensitive tests for experimental validation of fuel cell models. Notably, we consider effects of diffuse charge on electrochemical charge transfer rates by combining a generalized Frumkin-Butler-Volmer model for reaction kinetics across the compact Stern layer with the full Poisson-Nernst-Planck transport theory, without assuming local electroneutrality. Since this approach is rare in the literature, we provide a brief historical review. To illustrate the general theory, we present results for a monovalent binary electrolyte, consisting of cations, which react at the electrodes, and non-reactive anions, which are either fixed in space (as in a solid electrolyte) or are mobile (as in a liquid electrolyte). The full model is solved numerically and compared to analytical results in the limit of thin diffuse layers, relative to the membrane thickness. The spatial profiles of the ion concentrations and electrostatic potential reveal a complex dependence on the kinetic parameters and the imposed current, in which the diffuse charge at each electrode and the total membrane charge can have either sign, contrary perhaps to intuition. For thin diffuse layers, simple analytical expressions are presented for galvanic cells valid in all three (dis-)charging modes in the two subsequent limits of the ratio δ of the effective thicknesses of the compact and diffuse layers: (i) the "Helmholtz limit" ($\delta \to \infty$) where the compact layer carries the double-layer voltage as in standard Butler-Volmer models, and (ii) the opposite "Gouy-Chapman limit" ($\delta \to 0$) where the diffuse layer fully determines the charge-transfer kinetics. In these limits, the model predicts both reaction-limited and diffusion-limited currents, which can be surpassed for finite positive values of the compact-layer, diffuse-layer and membrane thicknesses.

Introduction

Reversible galvanic cells, such as redox flow cells [1]-[4], reversible solid oxide fuel cells [5]-[9], and rechargeable batteries [10]-[12] are electrochemical cells that can run both in a galvanic mode, thereby converting chemical energy in electric energy, and in the reverse, electrolytic, mode where electrical energy is returned into chemical energy. In the galvanic mode electrons flow spontaneously through an external load toward the more positive electric potential in the direction from anode to cathode, whereas in the electrolytic mode, the electrons are pumped toward the more negative potential of the cathode. Similar to rechargeable batteries, redox flow cells and reversible solid oxide fuel cells can be used to store electrical energy in the form of chemical energy. The main difference with rechargeable batteries is that the chemical energy is stored in a fluid phase which can be pumped to a secondary container, rather than being stored in a finite-capacity solid phase.

In this manuscript we develop a general mathematical model of electrochemical charge transfer and ion transport in galvanic cells and apply it to a one-dimensional model cell operating in steady state. We analyze not only the standard galvanic discharging regime in which the cell 'generates electricity' with positive power by spontaneously driving electrons through the external circuit [17][18], but also two operating regimes which require external electrical forcing. The first is the electrolytic charging regime in which an applied voltage exceeding the open-circuit voltage drives current in the reverse direction to convert electrical energy into chemical energy [5]-[9], while the second is an unconventional 'super-galvanic' regime in which the current is forced beyond the maximum for a galvanic cell in a shorted circuit. These three modes of operation are illustrated in Figure 1. Analysis of the full range of operation is important to better understand the efficiency and physical mechanisms of energy conversion, and to enable more sensitive experimental validation of mathematical models of galvanic cells.

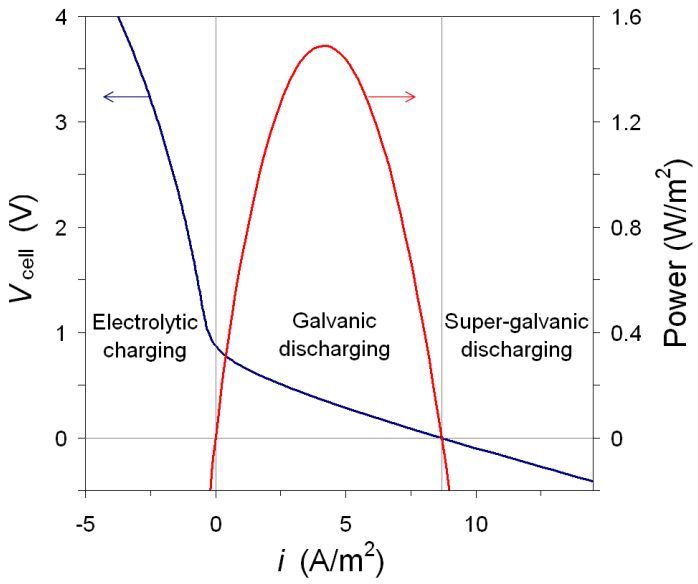

Fig. 1. Regimes of operation of a galvanic cell with imposed current. The calculations are based on a proton conducting fuel cell (see parameter settings of Fig. 3).

In this manuscript we will present calculation results for the ion density and electrostatic potential profiles as function of charge-transfer kinetic rates and of the imposed current. Two models for the electrolyte are considered. In the first case we consider a membrane electrolyte material in which the countercharge has a fixed, constant, distribution in space, while only the reactive ion is mobile. This is the typical situation for a solid-state proton or oxygen-ion conducting electrolyte membrane. In the second case we analyze the situation where the inert (non-reactive) ion is mobile and is redistributed across the membrane. This situation is more typical for a fuel cell or redox flow cell operating in liquid (e.g., aqueous) solution.

In both cases we illustrate the general theory in calculations that assume a one-dimensional planar geometry, steady-state operation, and constant (time-independent) chemical potentials of the reduced forms of the reactive cation, whose values are different at the anode and the cathode to describe a galvanic cell. The assumption of a constant chemical potential in each electrode corresponds, for instance, to a hydrogen fuel cell where the cation is a proton which reacts to/from an absorbed hydrogen atom in equilibrium with a large gas phase of constant hydrogen pressure (higher in the anode compartment than in the cathode compartment). The same assumption can also describe the case that the ion reduces to a neutral atom upon arriving at the cathode and is incorporated into the electrode phase (and vice-versa for oxidation at the anode). In this situation, our calculations extend the analysis of Bazant *et al.* [13]-[15] on electrolytic cells, where the reactions occurring at the two electrodes are the same, only driven in opposite directions by an applied cell voltage (and thus the open circuit voltage is zero). In such situations, the behavior of the model electrolytic cell is invariant with respect to the sign of the current, but this symmetry is broken in a galvanic cell because the conditions at the two electrodes are different.

An important element in our work is the consideration of diffuse charge, or polarization, effects near the electrodes. By including these effects in our calculations, we build on recent work for fuel cells [16][17] that goes beyond the standard assumption of electroneutrality throughout the electrolyte phase, which is ubiquitous in the battery and fuel-cell literature [5][11][18]-[27]. Though polarization of the electrolyte is confined to nanoscopic “diffuse charge” or “space charge” layers near the electrodes where ionic concentrations and the electrostatic potential rapidly vary, as shown in Fig. 2, the electrostatic potential across the polarization layer can be a significant part of the overall cell voltage. An additional reason to consider the polarization layer in detail is that the ion concentrations and field strength at the reaction plane (which we equate to the Stern, or Outer Helmholtz, plane, i.e. the boundary of the electrolyte continuum) strongly influence the electron charge transfer rate. We emphasize in this work the importance of a final “Stern” boundary condition, which relates the Stern layer voltage difference to the field strength at the Stern plane [13]-[15],[38]. Considering these elements jointly, a complete mathematical model is developed which self-consistently and logically describes the effect of the charge stored in the polarization layers on the electrochemical charge transfer rates. In contrast, in standard models for electrochemical cells, local electroneutrality is implicitly assumed throughout the complete electrolyte phase, and the electron charge-transfer rate does not depend on the structure of the polarization layer.

Polarization layer effects in electrochemical cells have been included in a limited amount of previous work [13]-[17],[28]-[30],[39],[40] but except for refs. [16][17] these papers consider electrolytic operation where the open-circuit voltage (OCV) is zero and no current is generated spontaneously upon closing the electrical circuit. This class of problems includes the broad topic of electrodialysis, where ion transport is analyzed between ion-exchange membranes under the application of an external voltage. Related work has focused on super-limiting currents and hydrodynamic instability at large voltages [31][32], but for this class of problems much simpler Dirichlet boundary conditions of constant ion concentrations and constant electrostatic potential are commonly used to describe the membrane-electrolyte interface. In the present context of Faradaic charge transfer reactions, some authors modeling diffuse charge in electrolytic cells [28][29] have simplified the problem by taking the Gouy-Chapman limit of a zero Stern layer thickness, but this removes any local field strength-dependence from the charge-transfer reaction rate and thus predicts a reaction-limited current, which cannot be exceeded without negative ion concentrations in the model. With a Stern layer included, it can be shown that ion concentrations are always positive [13][15]. In the case of a fuel cell with fixed countercharge, a more detailed galvanic cell model, which includes polarization layer effects, has been developed by Franco *et al.* [16].

In our recent paper [17] a fuel-cell model is presented for the case of fixed countercharge, where local electroneutrality *in the bulk electrolyte* is assumed and a quasi-equilibrium structure of the polarization layer considered. This is the thin diffuse layer ('thin-DL') limit of the full model presented below. In ref. [17] calculation results are presented, following Bazant *et al.* [14][15], as function of the parameter δ, the ratio of the effective Stern layer (or compact layer) thickness to the Debye screening length. In the "Gouy-Chapman limit" of $\delta=0$, the Stern-layer potential difference is zero, while in the opposite "Helmholtz limit", where $\delta=\infty$, the Stern layer carries the complete voltage across the double layer, since in the Helmholtz limit the Stern capacity is assumed to be infinitely larger than that of the diffuse layer. The Helmholtz limit of the generalized Frumkin-Butler-Volmer (gFBV) equation (discussed below in detail) turns out to be equivalent to the standard Butler-Volmer (BV)-based model for fuel cell operation [18]-[20],[22],[26],[27]. Therefore, in ref. [17] a mathematically simple methodology is presented to generalize the standard BV-model for fuel cells toward arbitrary values of the ratio δ. In the present work we build on refs. [16] and [17] by also considering mobile countercharge, by analyzing in more detail the structure and charge sign of the polarization layers as function of current, and by studying the effect of imposing negative and very positive currents on galvanic cell operation.

When ions can be considered as point charges, without excluded volume, the structure of the electrolyte including the diffuse (polarization) layer that forms on the electrodes is described using the full, non-equilibrium Poisson-Nernst-Planck (PNP) model for the transport rates of all mobile ions through the electrolyte [32]. At equilibrium, or in the thin-DL limit, the diffuse part of the double layer can be described by Poisson-Boltzmann (PB) theory (Gouy-Chapman equation). These microscopic models for the polarization layer must be coupled to a suitable expression for the electron charge transfer rate and combined with an additional boundary condition on the electrostatic potential, to replace the macroscopic assumption of bulk electroneutrality. Here we will use a generalized Frumkin-

corrected Butler-Volmer (gFBV) equation which, in our view, extends in a relevant way more familiar formulations based on the assumption of local equilibrium of the polarization layer. The gFBV-formulation explicitly considers the compact (or Stern) layer potential difference as the driving force for electron transfer and the concentrations of reactive ions directly adjacent to the electrode, i.e., at the Stern or reaction plane, and does not a-priori assume the existence of a quasi-equilibrium Boltzmann distribution of the polarization layer. For the additional electrostatic boundary condition, we model the Stern layer as a uniform dielectric, and this effectively gives the forward and backward reaction rates an Arrhenius dependence on the normal electric field at the electrode. The generalized formulation completes the mathematical description without arbitrary assumptions such as local equilibrium or electroneutrality of the electrolyte or for instance a prescribed, constant surface charge, and can be applied in such situations as thin electrolyte films (where diffuse layers overlap and/or the bulk electrical field is a significant portion of the field strength in the polarization layer), operation at large, super-limiting currents [15] or large AC frequencies, which are all situations where the diffuse charge distribution loses its quasi-equilibrium structure.

FBV-formulations for the charge-transfer rate (either generalized, and those that assume quasi-equilibrium for the polarization layers) differ from the standard unmodified BV-approach in which the ion concentrations outside the polarization layer (in the quasi-neutral bulk solution) are used and the interfacial overpotential is based on the total potential difference across the interface (thus over the Stern layer plus the diffuse layer) or more heuristically is based on the electrode potential relative to that of a reference electrode. When the BV equation is used, one is forced to combine this with a model for ion transport that neglects the possibility of charge separation (as occurs in the polarization layer). Instead, the gFBV equation which is based on local conditions at the Stern plane (ion concentration, and field strength, which determines the Stern layer potential difference) can be unequivocally and transparently combined with the PNP model which describes ion concentration and potential profiles both in the electrolyte bulk, as well as in the diffuse layers, all the way up to the reaction planes. The resulting PNP-gFBV model can be generally used, for the equilibrium situation, as well as for steady-state and fully dynamic transport problems.

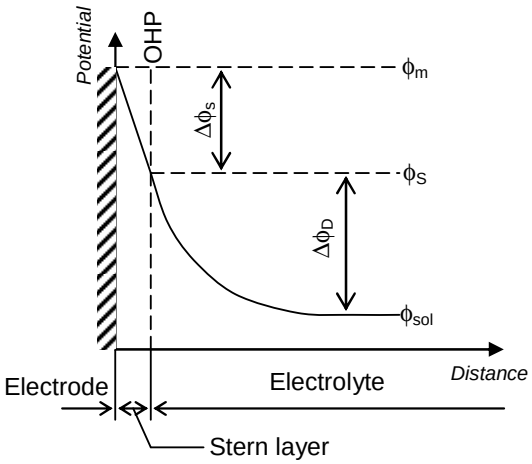

Fig. 2. Schematic representation of potentials in an equilibrium polarization layer based on the Gouy-Chapman-Stern model, in which the compact or Stern layer is located directly next to the electrode and separated from the diffuse layer (and ultimately the electrolyte bulk solution) by the Stern, reaction, or Outer Helmholtz plane (OHP).

History of modeling electrochemical charge transfer including polarization-layer effects

The mathematical description of charge-transfer reactions is at the heart of any model for electrochemical cells, so we begin with a brief historical overview of various contributions where polarization-layer effects are included in charge-transfer rate modeling, a development initiated by Frumkin [33] who first included diffuse-charge effects in a Butler-Volmer framework. In this section we describe what we call the "generalized Frumkin-Butler-Volmer" (gFBV) equation, and compare with related representations in the literature. The gFBV-equation for the electrochemical conversion rate J of an n-electron reaction is given as a sum of an oxidation and a reduction reaction

$$J = K_O C_R \exp\left(\alpha_O n \Delta\phi_s\right) - K_R C_O \exp\left(-\alpha_R n \Delta\phi_s\right) \tag{1}$$

where α_O and α_R are the transfer coefficients ($\alpha_O+\alpha_R=1$) and C_R and C_O are concentrations of the reacting species in the reduced and oxidized state at the Stern, pre-electrode, Outer-Helmholtz, or reaction, plane [in numbers per volume]. As we will explain in more detail below, Eq. (1), although superficially similar, is fundamentally at odds with the textbook literature in electrochemistry, because $\Delta\phi_s$ is here explicitly defined as the voltage difference across the inner, or Stern, layer and concentrations are those at the Stern, or reaction, plane, not outside the polarization layer. In Eq. (1) we have assumed ideal thermodynamics for the two atoms (or, ions) "R" and "O" and use concentrations C_i instead of activities, a_i. Non-idealities, such as volume constraints for finite-sized ions, can be included in modifications of Eq. (1), such as discussed in ref. [17]. More general models based on electrochemical potentials for non-ideal solutions have also recently been proposed in the context of rechargeable batteries [12] but here we focus on the traditional Butler-Volmer perspective, where the interfacial voltage biases the energy barrier for charge transfer.

In particular, in Eq. (1), we view $\Delta\phi_s$ as the difference in dimensionless electrostatic potential between the electrode, ϕ_m, and the electrical potential at the reaction, plane, ϕ_S, which is usually assumed to coincide with the Stern plane, just beyond the first solvation layer of the electrode [34]. To simplify notation, throughout the paper we use dimensionless electrostatic potentials ϕ which relate to dimensional potentials V via $\phi=f\cdot V$ with $f=F/RT=e/kT$ is the inverse thermal voltage. The conversion rate J relates to the Faradaic current density i according to $i=J\cdot e\cdot n$.

For the one-electron proton reduction, Frumkin [33] already gives Eq. (1) [first part of his Eq. (3) for the proton reduction, and his Eq. (4) for the oxidation]. Also for the one-electron proton reduction and the reverse oxidation, Eq. (1) is given by Levich [35]. For an n-electron reduction, the second part of Eq. (1) is also given as Eq. (56) by Parsons [36]. For infinitely fast kinetics, the appropriate electrochemical boundary condition can also be derived from Eq. (1). Assuming C_R fixed, e.g. for an ion that upon reduction becomes incorporated in the electrode, Eq. (1) results for n=1 in $\Delta\phi_s = \beta + \ln C_O$ with β a constant. This boundary condition was used in numerical work by Buck [37] (his Eq. 6) and Smith and White [32]. Itskovich *et al*. [38] give Eq. (1) for a one-electron reaction with C_R fixed (their Eq. (10), based on assuming a constant chemical potential of the species in the reduced state), given by

$$J = J_* \left[\exp(\alpha_O \eta) - \frac{C_O}{C_{O,eq}} \exp(-\alpha_R \eta) \right] \tag{2}$$

where the 'Stern' overpotential η is the potential difference across the Stern layer minus that value at equilibrium, given by $\eta = \Delta\phi_s - \Delta\phi_{s,eq}$. We can show that Eq. (2) directly results from Eq. (1) when we set J=0 in Eq. (1) to obtain the equilibrium potential over the Stern layer, $\Delta\phi_{s,eq}$, as $\Delta\phi_{s,eq} = \ln \frac{K_R C_{O,eq}}{K_O C_{R,eq}}$, where $C_{O,eq}$ and $C_{R,eq}$ are the concentrations of the oxidized and reduced species at equilibrium at the Stern plane, and by making the replacements $J_* = \left(K_R C_{O,eq}\right)^{\alpha_O} \left(K_O C_{R,eq}\right)^{\alpha_R}$.

For completeness we give the generalized n-electron version of Eq. (2) with also C_R participating, which is given by

$$J = J_* \left[\frac{C_R}{C_{R,eq}} \exp(\alpha_O n \eta) - \frac{C_O}{C_{O,eq}} \exp(-\alpha_R n \eta) \right] \tag{3}$$

where as above concentrations C are defined at the Stern plane, and the Stern overpotential η is given by $\eta = \Delta\phi_s - \Delta\phi_{s,eq}$. Finally we represent Eq. (1) as

$$J = J^\dagger \left[C_R \exp\left(\alpha_O n \left(\Delta\phi_s - \phi^0\right)\right) - \frac{C_O}{C_{O,eq}} \exp\left(-\alpha_R n \left(\Delta\phi_s - \phi^0\right)\right) \right] \tag{4}$$

where ϕ^0 is a 'formal potential', which follows from Eq. (1) as $\phi^0 = n^{-1} \cdot \ln\left(K_R K_O^{-1}\right)$ and where $J^\dagger$ is given by $J^\dagger = K_R{}^{\alpha_O} K_O{}^{\alpha_R}$. Eq. (4) was given for n=1 in refs. [39] and [40].

Equation (1) has been written down in some recent papers and analyzed with different, simplified models of the double layer. In the context of charge transfer between two immiscible electrolyte solutions, Horvai [44] gives Eq. (1) but with n replaced by z, being the 'charge of the ion'. In the same context, Senda [45] exactly gives Eq. (1) for an n-electron reaction. Murphy *et al.* [28] give a representation of Eq. (1) for a one-electron reaction with the concentration of both the oxidized and reduced species included, which is their Eq. (15). To our knowledge, ref. [28] is the first paper that makes a full numerical calculation of a complete electrochemical cell with a microscopic reaction model, which is a limit of the gFBV equation (1), combined with the full Poisson-Nernst-Planck (PNP) transport theory. In their calculations, Murphy *et al.* [28] only consider the Gouy-Chapman (GC) limit of the gFBV equation (effectively setting $\Delta\phi_s$=0) because the "ions are assumed to be point charges... and the plane of closest approach of ions is just the electrode surface." A similar exercise, in which the PNP theory is combined with the gFBV equation in the GC-limit, is presented by Moya *et al*. [29]. In both papers the kinetic constants are chosen such that at equilibrium no polarization layer is formed, and thus the OCV is zero. The electrostatic boundary condition used in these papers [28][29] essentially equates the potential at the reaction plane to that of the electrode under all conditions. This GC-limit ($\Delta\phi_s$=0), however, lacks any voltage or electric-field dependence and thus reduces to standard first-order chemical reaction kinetics and can also become unphysical in some situations, since it predicts reaction-limited currents, beyond which negative ion concentrations are predicted. As we shall see, this problem can be avoided by introducing a more general boundary condition on the

electrostatic potential, which self-consistently inserts the electric field dependence in the reaction rate via the full gFBV equation (1).

Superficially similar expressions as Eqs (1)-(4) can be found in the textbook literature (e.g., see p. 99 in ref. [41]; p. 210 in ref. [42]; p. 109 in ref. [43]) but there presented without inclusion of polarization layer effects (standard Butler-Volmer equation) and thus with the concentrations, C_i, defined outside the diffuse layer, and the overpotential, η, defined as the difference between the case with and without current of the potential difference across the full polarization layer, from electrode to solution. Even more heuristically, the overpotential is often defined as the measurable difference between the situation with and without current of the working electrode potential relative to that of reference electrode. This approach, to omit polarization layer effects in the modeling of charge-transfer reactions, may be due to the perspective, summarized by Newman [42], that microscopic double layer modeling lacks a "firm macroscopic basis" in thermodynamics, and thus "cannot be applied with any certainty to solid electrodes", in spite of the "impressive qualitative account of complicated electrode behavior that can be attributed to double layer structure". For thin diffuse layers, Newman attributes this uncertainty to the unknown surface charge, which would be enough to determine the ion profiles in quasi-equilibrium (unaffected by the current).

From a mathematical perspective, what is missing is a microscopic boundary condition on the electrostatic potential, which can provide the local field strength entering the gFBV equation (1). Indeed, we are not aware of any textbooks on electrochemistry that provide a complete set of boundary conditions for microscopic modeling with diffuse charge, since the assumption of bulk electroneutrality obviates the need for a boundary condition on the potential. Instead, the standard approach for microscopic modeling within the polarization layer is simply to specify the surface charge, ion concentration or potential (usually equated with the electrokinetic "zeta potential"). Below, we will show that all of these parameters (surface charge, concentration, potential) can be highly sensitive to the current and reaction parameters in a complete microscopic model, and thus cannot be left as a macroscopic fitting parameter without sacrificing predictability.

To our knowledge, the "missing boundary condition" on the electrostatic potential to be used in conjunction with the generalized, non-equilibrium, FBV equation (1) was first proposed to be explicitly related to the properties of Stern's compact layer by Itskovich *et al*. [38]. We are not aware of any subsequent work with this general mathematical model for charge-transfer reaction kinetics with diffuse charge until the recent work of Bazant *et al.* [13]-[15],[46] who write the electrostatic boundary condition at the Stern plane in the form

$$\left.\frac{\mathrm{d}\phi}{\mathrm{d}X}\right|_{\mathrm{S}} = \mp\frac{\Delta\phi_{\mathrm{s}}}{\lambda_{\mathrm{S}}} \tag{5}$$

where X is the place coordinate, and λ_S is an effective width for the compact layer, equal to its true width times the permittivity ratio of the electrolyte to the compact layer. In Eq. (5) and subsequent expressions, the upper sign in '$\pm$' and '$\mp$' is required for boundaries where the position coordinate X points from electrode into the electrolyte (in our calculations this will be the anode side), and the lower sign is for the other electrode. The boundary condition, Eq. (5), enforces continuity of the electric displacement from the continuum electrolyte region into the compact layer, which is described by

Stern's model of an uncharged, uniform dielectric coating on the electrode. As described in ref. [14], Eq. (5) can also be generalized to account for a nonlinear, charge-dependent differential capacitance of the Stern layer. The combination of the gFBV equation (1) with the Stern boundary condition, Eq. (5), yields an intuitive expression for charge-transfer reaction kinetics,

$$J = K_O C_R \exp(\mp\alpha_O n\lambda_S \phi'_{\mathbf{n}}) - K_R C_O \exp(\pm\alpha_R n\lambda_S \phi'_{\mathbf{n}}) \qquad (6)$$

where the acceleration factor of the kinetic rates is shown to be proportional to the normal electric field strength at the reaction plane; for a one-dimensional geometry, $\phi'_{\mathbf{n}} = \left.\frac{\mathrm{d}\phi}{\mathrm{d}X}\right|_S$.

Eq. (6) clearly shows the departure of the generalized FBV formulation from the traditional BV approach: whereas in the latter the driving force (the term within the exponent) is the overpotential η, i.e., a difference in potential between two positions (electrode and solution, or between the working and reference electrode) and two conditions (with non-zero and zero current), here it (simply) is a fully local property only requiring information of the present state (not requiring comparison with the equilibrium state), namely the *gradient* of potential at the Stern plane. Not only are we of the opinion that this is the more general result, but additionally also that it is a much more insightful and easier-to-grasp formulation of how the electrode potential influences charge-transfer rates. It can be transparently incorporated in general calculation schemes for electrochemical systems as a fully 'localized' boundary condition, without a need to consider reference and equilibrium states, etc.

A crucial dimensionless group in the full PNP-gFBV description is the ratio δ of the effective thickness of the Stern layer λ_S to that of the diffuse layer λ_D given by the Debye-Hückel screening length, first introduced as the parameter γ by Itskovich *et al.* [38]. The influence of (non-zero values for) δ was investigated in detail only much more recently, starting with Bonnefont *et al.* [13] using a complete PNP-gFBV description including the Stern boundary condition. (Itskovich *et al.* [38] only analyze single-electrode polarization curves.) Bonnefont *et al*.'s [13] Eq. (7) is equivalent to our Eq. (1) (but note the reversed subscripts "R" and "O"). Furthermore, Bonnefont *et al*. [13] are first to take values of the ratio K_O/K_R such that at equilibrium a polarization layer is formed, but since this ratio is the same on both electrodes, the open-circuit voltage, OCV, equals zero, which precludes spontaneous current and only describes electrolytic cell operation. Bazant *et al.* [14], Chu and Bazant [15] and Prieve [30] extend these calculations. He *et al.* [39] use the gFBV-formulation in the represention of Eq. (4), for a steady-state calculation for a spherical nanoelectrode, with the counterelectrode as a infinitely large shell, infinitely far away. On the nanoelectrode they set the formal potential ϕ^0 to zero which implies that at equilibrium no polarization layer is formed. The same gFBV-representation is used in ref. [40]. In both these works a seemingly rather complicated expression is used for the potential drop over the compact layer, $\Delta\phi_S$, which however, is equivalent to Eq. (5). Olesen *et al*. [47] also give Eq. (1) for a one-electron reaction but in their calculations take a local equilibrium approach for the polarization layer, and linearize for a small Stern overpotential. In the context of proton-conducting fuel cell modeling, the gFBV equation was recently given by Franco *et al.* [16] (his Eq. (52)) in a fully dynamic transport model, an approach which was significantly simplified in ref. [17] assuming local equilibrium for the polarization layers.

Interestingly, this generalized formulation, which was the starting point of Frumkin's analysis [33], in which the ion concentrations are taken at the Stern plane, and the potential driving the electron transfer is explicitly based on the Stern layer potential difference, is rarely mentioned in the literature, let alone used in calculations. (To our knowledge, the above literature overview is rather complete.) Instead, starting with Frumkin himself in 1933, the polarization layer structure has always been considered to be locally at equilibrium, and this additional information has been implemented [48]. This is surely a suitable simplification in many cases, although it has more limited predictive power, because it breaks down when polarization layers influence one another such as when the electrolytic film is thin, electron currents are very high and/or large AC frequencies are applied. Another important point is that the resulting expressions do not necessarily become easier to grasp.

Let us show that Eq. (1) is equivalent to the resulting more common representations of the Frumkin-Butler-Volmer equation, which we base on Eq. (11) in Delahay [49] (p. 158), given by

$$i = i_t^0 \exp\left\{(\alpha n - z)\phi_2\right\}\left[\exp\left\{-\alpha n\left(\phi_M - \phi_M^e\right)\right\} - \exp\left\{(1-\alpha) n\left(\phi_M - \phi_M^e\right)\right\}\right] \tag{7}$$

where i_t^0 is an exchange current density, z the charge of the oxidized ion, ϕ_M is the dimensionless electrode potential with reference to the bulk of the solution outside of the double layer (ϕ_{sol}), and ϕ_M^e the value of ϕ_M at equilibrium (for zero current); ϕ_2 is the potential at the reaction plane, also relative to ϕ_{sol}, see Fig. 2. Replacing in Eq. (7) ϕ_M-ϕ_2 by $\Delta\phi_s$, $\exp(-z\cdot\phi_2)$ by $C_O/C_{O,\infty}$ (this is where we remove the equilibrium Boltzmann assumption again and return to the generalized formulation), replacing the constants $i_t^0\cdot\exp(\alpha n\phi_M^e)/C_{O,\infty}$ by K_R, $\exp(-(z-n)\cdot\phi_2)$ by $C_R/C_{R,\infty}$ (Boltzmann for the reduced species), and replacing $i_t^0\cdot\exp(-(1-\alpha)n\phi_M^e)/C_{R,\infty}$ by K_O, we obtain Eq. (1) (apart from an overall minus-sign; note that $\alpha=\alpha_R$ and $1-\alpha=\alpha_O$).

Besides its more general applicability, an additional advantage of Eq. (1) over Eq. (7) is in our view its increased transparency, for instance showing clearly the role of ion concentrations in the charge transfer rate, not being hidden in the parameters ϕ_M^e and i_t^0. A related point is that the representation according to Eq. (7) implicitly requires unchanging and unambiguous values for the background ion concentrations, $C_{O,\infty}$ and $C_{R,\infty}$. Though this requirement will be valid in many situations, at high currents and/or thin electrolyte films significant gradients in ion concentration can develop in the bulk electrolyte when all ions are mobile, and $C_{O,\infty}$ and $C_{R,\infty}$ are then different at the anode and cathode. For very high currents a related effect is that the polarization layer expands significantly [15],[31],[50] no longer conforming to the (Gouy-Chapman) equilibrium structure, which can also be the case when high frequencies are applied in the voltage or current signal imposed on the electrochemical cell.

Theory

In this section we discuss the complete mathematical model, which combines the Poisson-Nernst-Planck (PNP) model for the ion transport flux in the electrolyte with the generalized Frumkin-Butler-Volmer (gFBV) rate equation and the Stern boundary condition. The theory can be generally applied both for the case where the countercharge is mobile and for the case where it is immobilized, such as will be assumed in an example calculation for a solid electrolyte used in a hydrogen fuel cell. In the latter case, an overall balance for the inert ions does not need to be considered. At the end of this

section we first discuss the simplifications that result in the thin diffuse layer (thin-DL) model of ref. [17] and finally present the analytical results when additional to the thin-DL assumption, the GC-limit (δ=0) or Helmholtz-limit (δ=∞) is considered as well, both for the case of mobile and for immobilized countercharge. Note that throughout this manuscript we focus on a one-dimensional and planar geometry, with two perfectly smooth, planar electrodes placed perfectly parallel, in direct contact with the electrolyte phase in between, which only contains the reactive monovalent cations and inert monovalent anions. Effects of additional background salt are not considered [32]. Because we only consider the steady state, the charge transfer rate J is equal to the electron current density i (when J is multiplied with the electronic charge e and the number n), as well as being equal to the transport flux of the reactive ion (being the cation), at each position in the electrolyte. Note that in a dynamic (time-dependent) calculation this would be different and the Maxwell displacement current, related to capacitive charging of the double layers, would have to be included as well [13],[28],[29],[46].

Electrochemical charge transfer and equilibrium thermodynamics

In the calculations we assume a one-electron reaction $O^+ + e^- \leftrightarrow R$ with R being a neutral particle at a fixed chemical potential. This condition is appropriate for a system where the neutral particle derives from the electrode, e.g. as in electro-dissolution of a metal [13]-[15], or because it is an absorbed neutral hydrogen atom in equilibrium with hydrogen molecules in an adjacent gas phase [17]. In those cases, Eq. (1) simplifies to

$$J = J_O \exp\left(\tfrac{1}{2}\Delta\phi_s\right) - K_R C_O \exp\left(-\tfrac{1}{2}\Delta\phi_s\right) \tag{8}$$

where we have also assumed the transfer coefficients to be equal to ½. (See references in ref. [14] on the appropriateness of assuming α=½ for one-electron reactions, and see ref. [51] where it is argued that when experimentally deviations from α=½ are observed, this may well be due to neglected polarization-layer effects.) The transfer rate J is defined to be positive for the oxidation reaction, which implies that when cations are the only reactive species in the electrolyte, it describes the cation flux in the direction away from the electrode into the electrolyte. (Note that this is the opposite of the sign convention in refs. [13]-[15].) The rate constants K_R and J_O for the reduction and oxidation together fully define both the kinetics and the thermodynamics of the charge transfer reaction (both numbers are strictly positive). Indeed, from the gFBV equation we can derive how the rate constants K_R and J_O relate to the thermodynamics of the process, especially to the electromotive force, or open circuit voltage, ϕ_0. Assuming J=0 and implementing a Boltzmann distribution, $C_O = C_\infty \exp\left(-\Delta\phi_D\right)$, which is valid in the limit of thin, non-overlapping double layers (where the electric field is negligible outside the double layer, compared to the larger values within), we obtain from Eq. (8) the Nernst equilibrium condition for the electrode potential [33][52],

$$\Delta\phi_T = \ln\frac{K_R C_\infty}{J_O} = \text{cnst} + \ln C_\infty \tag{9}$$

where $\Delta\phi_T$ is the total interfacial potential difference over the double layer (thus, across Stern plus diffuse layer), counted from electrode to bulk solution ($\Delta\phi_T=\phi_m-\phi_{sol}$).

For a full electrochemical cell at equilibrium, the potential difference over the bulk electrolyte solution is zero, and thus the dimensionless open cell voltage $\phi_0 = \phi_{m,C} - \phi_{m,A}$ is given by

$$\phi_0 = \Delta\phi_{T,C} - \Delta\phi_{T,A} = \ln\frac{K_{R,C}}{K_{R,A}}\frac{J_{O,A}}{J_{O,C}} \tag{10}$$

where A and C refer to the anode and cathode. Because we define ϕ_0 to be positive for galvanic operation, we must choose the anode and cathode such that we comply with $K_{R,C}/J_{O,C} > K_{R,A}/J_{O,A}$.

Poisson-Nernst-Planck transport model

The Nernst-Planck equation describes the mass transfer flux of each of the ionic species as a sum of a concentration term (diffusion) and a term due to the electrical field (migration),

$$J_i = -D_i\left\{\frac{dC_i}{dX} + z_i C_i \frac{d\phi}{dX}\right\} \tag{11}$$

where D_i is the ion diffusion coefficient, z_i the dimensionless charge (e.g. -1 for a monovalent anion), and X the place coordinate. For a solid electrolyte with fixed anions, we set $D_-=0$. For a complete description of the electrolyte phase, Eq. (11) must be supplemented with Poisson's equation

$$\frac{d^2\phi}{dX^2} = -4\pi\lambda_B \cdot \left(C^+ - C^-\right) \tag{12}$$

where λ_B is the Bjerrum length, given by $\lambda_B = e^2/(4\pi\varepsilon kT)$, which can be related to the Debye-Hückel screening length according to $\lambda_D = (8\pi\lambda_B C_\infty)^{-1/2}$.

For stationary conditions (steady-state), and a planar, one-dimensional geometry, the flux J is everywhere the same for the reactive species, and at the boundaries (reaction planes) it is (in magnitude) equal to the Faradaic current given by Eq. (8). In steady state, the flux is zero everywhere for the inert ions. The final boundary condition is provided by the Stern condition, Eq. (5). Following ref. [14], one more condition is needed to relate the current to the cell voltage in steady state, which is an integral constraint specifying the total number of inert anions

$$\int_0^L C_i dX = C_\infty \cdot L \tag{13}$$

where C_∞ is the average concentration of inert anions. For a 1:1 salt, with one ion reactive and the other inert (without added indifferent salt), C_∞ equals the bulk ionic strength.

Dimensionless Poisson-Nernst-Planck Frumkin-Butler-Volmer model

Next we discuss the dimensionless representation of the full PNP-gFBV model based on a system with a monovalent reactive cation, and a single type of monovalent inert anion. First we present the model for the case that the inert ion is fixed in space, at a constant concentration of C_∞. The dimensionless coordinate is given by x, running from anode to cathode, related to the dimensional coordinate X according to $x=X/L$ where L is the distance between the two opposite Stern planes. The ratio of Stern layer thickness over Debye length is given by $\delta=\lambda_S/\lambda_D$ and the ratio of λ_D over L is given by ε, i.e., $\varepsilon=\lambda_D/L$. The dimensionless concentration of the cationic mobile species is c^+, which is the dimensional concentration C^+ over C_∞. The dimensionless Poisson equation then becomes

$$\frac{\mathrm{d}^2\phi}{\mathrm{d}x^2} = -\frac{1}{2\varepsilon^2}\cdot\left(c^+ - 1\right) \tag{14}$$

while the dimensionless Nernst-Planck equation in the steady-state becomes

$$\frac{\mathrm{d}c^+}{\mathrm{d}x} = -4\cdot j - c^+\frac{\mathrm{d}\phi}{\mathrm{d}x} \tag{15}$$

where the reduced flux j is given by $j=J/J_{\mathrm{lim}}$ with $J_{\mathrm{lim}}=4\cdot D_+\cdot C_\infty/L$ [13]-[15].

The dimensionless gFBV equation is given by

$$\pm j = j_{\mathrm{O}}\exp\left(\tfrac{1}{2}\Delta\phi_{\mathrm{s}}\right) - k_{\mathrm{R}}c_{\mathrm{O}}\exp\left(-\tfrac{1}{2}\Delta\phi_{\mathrm{s}}\right) \tag{16}$$

where $k_{\mathrm{R}} = \frac{K_{\mathrm{R}}C_\infty}{J_{\mathrm{lim}}}$ and $j_{\mathrm{O}} = \frac{J_{\mathrm{O}}}{J_{\mathrm{lim}}}$. At the two Stern planes the boundary condition is

$$\Delta\phi_{\mathrm{s}} = \mp\varepsilon\delta\left.\frac{\mathrm{d}\phi}{\mathrm{d}x}\right|_{\mathrm{S}}. \tag{17}$$

When both ions are mobile, Eq. (14) is modified to

$$\frac{\mathrm{d}^2\phi}{\mathrm{d}x^2} = -\frac{1}{2\varepsilon^2}\cdot\left(c^+ - c^-\right) \tag{18}$$

and the Nernst-Planck equation must be solved for the anion as well, which becomes analogous to Eq. (15)

$$\frac{\mathrm{d}c^-}{\mathrm{d}x} = c^-\frac{\mathrm{d}\phi}{\mathrm{d}x} \tag{19}$$

and implies a Boltzmann distribution, $c^- \propto \exp(\phi)$, for thermal equilibrium in a dilute solution.

To simplify the analysis [13]-[15],[46], it is in this case (when both ions are mobile) advantageous to define an average dimensionless concentration $c=\frac{1}{2}\cdot(c^+ + c^-)$ and a dimensionless charge density $\rho=\frac{1}{2}\cdot(c^+ - c^-)$ which modifies Eq. (18) into

$$\frac{\mathrm{d}^2\phi}{\mathrm{d}x^2} = -\frac{\rho}{\varepsilon^2} \tag{20}$$

and results in a replacement of Eq. (15) and (19) by

$$\frac{\mathrm{d}c}{\mathrm{d}x} = -2\cdot j - \rho\frac{\mathrm{d}\phi}{\mathrm{d}x} \tag{21}$$

and

$$\frac{\mathrm{d}\rho}{\mathrm{d}x} = -2\cdot j - c\frac{\mathrm{d}\phi}{\mathrm{d}x}. \tag{22}$$

The model is completed with an overall balance for the inert ion, given by $\int_0^1 (c-\rho)\,\mathrm{d}x = 1$. Electrostatic potentials can be set to zero at an arbitrary position (in Figs. 5 and 6 the anode potential, $\phi_{\mathrm{m,A}}$, is set to zero, whereas $\phi_{\mathrm{m,C}}=0$ in Figs. 8 and 9).

Next we will discuss the analytical solution of the steady-state galvanic cell model in the asymptotic limit of thin-diffuse layers $\varepsilon\to 0$, where the membrane thickness is much larger than the Debye length. These equations can be used in all three modes of operation identified in Fig. 1. First we show the results for the case of fixed countercharge ('solid electrolyte') and secondly for mobile countercharge

('liquid electrolyte'). In the first case, this analytical model has already been presented in ref. [17] and will be repeated briefly here. For the case of mobile countercharge, this set of equations extends on the analytical model for an electrolytic cell in the thin-DL limit of ref. [14].

Galvanic cell model for the thin diffuse layer-limit for a solid electrolyte

In the thin diffuse layer-limit for a material with fixed countercharge, the Nernst-Planck equation, Eq. (11), can be simplified by neglecting the concentration diffusion term for bulk electrolyte transport, resulting in Ohm's law for ion transport, which for the case that only the cation is mobile and reactive, and for a one-dimensional planar geometry, is given by

$$i = R_{\text{elyt}}^{*\,-1} \cdot \Delta\phi_{\text{elyt}} \tag{23}$$

where i is the current density (in A/m^2) which equals the cation flux J times electron charge e, where $R_{\text{elyt}}^{*} = L \cdot \left(D_{+} C_{\infty} e\right)^{-1}$ (with L is membrane thickness) is an Ohmic resistance in m^2/A, and where $\Delta\phi_{\text{elyt}}$ is the dimensionless potential difference over the bulk electrolyte from a position just outside the diffuse layer at the anode-side of the cell to the same position on the cathode-side, $\Delta\phi_{\text{elyt}}=\phi_{\text{sol,A}}-\phi_{\text{sol,C}}$.

In the model in the thin-DL limit, an equilibrium structure for the diffuse layers prevails on each electrode, which are separated by the bulk electrolyte phase in which the concentration of ions is constant, namely the ionic strength C_∞. In this case we have Boltzmann statistics for the proton concentration at the Stern plane,

$$C_{\text{O}} = C_{\infty} \exp\left(-\Delta\phi_{\text{D}}\right) \tag{24}$$

where $\Delta\phi_{\text{D}}$ is the potential difference across the diffuse layer, equal to $\phi_{\text{S}}-\phi_{\text{sol}}$, with ϕ_{sol} the value of the potential outside the diffuse layer, at the start of the bulk solution phase.

In ref. [17] a modification of Eq. (8) was used that more explicitly considers a hydrogen concentration cell. In such a cell, protons migrate through the electrolyte, driven by a difference in the hydrogen gas pressure between the anode and cathode compartment. The calculation is based on an anode compartment with hydrogen gas pressure $p_{\text{H2,A}}$, and a cathode compartment with pressure $p_{\text{H2,C}}$ ($<p_{\text{H2,A}}$). In this case, when mass transport of gaseous hydrogen from the compartment to the electrodes, and the hydrogen dissociation reactions are fast enough, we can make the replacements $K_{\text{R}}=k^*_{\text{j}}\cdot\sqrt{p^*}/(C_\infty\cdot e)$ and $J_{\text{O}}=k^*_{\text{j}}\cdot\sqrt{p_{\text{H2}}}/e$, and together with Eq. (24) rewrite Eq. (8) as [17]

$$i = k^*_{\text{j}} \left\{\sqrt{p_{\text{H2}}} \exp\left(\tfrac{1}{2}\Delta\phi_{\text{s}}\right) - \sqrt{p^*} \exp\left(-\Delta\phi_{\text{D}} - \tfrac{1}{2}\Delta\phi_{\text{s}}\right)\right\} \tag{25}$$

where k^*_{j} is a purely kinetic rate constant of the respective electrode and p^* is a thermodynamic property of the membrane electrolyte material in combination with the electrode material (p^* has dimension of pressure). The parameter p^* can be considered the 'zero-charge pressure', i.e., is defined such that no polarization layer is formed at equilibrium in the membrane electrolyte when the hydrogen gas phase pressure in the adjacent compartment, p_{H2}, exactly equals p^*. For $p_{\text{H2}}>p^*$ the membrane electrolyte becomes positively charged at equilibrium, and vice-versa for $p_{\text{H2}}<p^*$.

For the equilibrium structure of the diffuse layer, the analytical solution for the case that the mobile ions are positive (cations) and the fixed anions are immobile, is given by [17],[53]

$$\Delta\phi_s = \frac{\Delta\phi_D}{|\Delta\phi_D|}\delta\sqrt{\exp(-\Delta\phi_D)+\Delta\phi_D-1}\,. \tag{26}$$

The model for the thin-DL limit is based on the above equations, evaluated on both electrodes, as well as on the closure equation

$$f\cdot V_{cell}=\phi_{cell}=\phi_{m,C}-\phi_{m,A}=(\Delta\phi_s+\Delta\phi_D)_C-(\Delta\phi_s+\Delta\phi_D)_A-\Delta\phi_{elyt}\,. \tag{27}$$

Recall that $f = F/RT = e/kT$ is the inverse of the thermal voltage used to define all of our dimensionless potentials. It must be noted that in this model based on the thin DL-limit where local "quasi-equilibrium" can be assumed in the diffuse layers, as described by Eq. (26), this does not imply that the structure of the diffuse layers is that of a true equilibrium system (where the current is zero). Instead, the electrode charge density and the values of $\Delta\phi_s$ and $\Delta\phi_D$ in Eq. (26) are influenced by the current density i via the gFBV equation, Eq. (25).

Note that Eqs. (23)-(25) can be rewritten in the dimensionless parameters as used in Eqs. (14)-(22) when we use the conversions $j_{O,i}=¼\cdot k^*_i\cdot R^*_{elyt}\cdot\sqrt{p}_{H2,i}$, $k_{R,i}=¼\cdot k^*_i\cdot R^*_{elyt}\cdot\sqrt{p^*}$, and $i=4\cdot j/R^*_{elyt}$, resulting in $\Delta\phi_{elyt} = 4j$ and $\pm j = j_O\exp(½\Delta\phi_s) - k_R\exp(-\Delta\phi_D - ½\Delta\phi_s)$.

We are now ready to derive analytical current-voltage relations for galvanic cells applicable in all three modes identified in Fig. 1. These relationships are based on first taking the thin-diffuse layer limit as above and then either the Gouy-Chapman limit (δ=0) or the Helmholtz-limit (δ=∞). For the GC-limit, we obtain

$$\phi_{cell} = \phi_0 - 4\cdot j + \ln\frac{1-j/j_{O,A}}{1+j/j_{O,C}} \tag{28}$$

where the dimensionless open cell voltage is $\phi_0 = \ln\left(\frac{k_{R,C}j_{O,A}}{k_{R,A}j_{O,C}}\right)$, while for the H-limit we obtain

$$\phi_{cell} = \phi_0 - 4\cdot j - 2\cdot\operatorname{arcsinh}\frac{j}{\sqrt{\beta_A}} - 2\cdot\operatorname{arcsinh}\frac{j}{\sqrt{\beta_C}} \tag{29}$$

where $\beta_A = 4\cdot k_{R,A}j_{O,A}$ and $\beta_C = 4\cdot k_{R,C}j_{O,C}$. Eqs. (28) and (29) are mathematically identical to the same limits of the thin-DL fuel-cell model presented in ref. [17] (Eqs. (25) and (27) there), using the conversions given above. The expression for the H-limit, Eq. (29), has been presented in the context of hydrogen fuel cells in refs. [18]-[20], [22], [26] and [27]. Results of the thin-DL model are plotted in Fig. 3a and compared to analogous expressions for the liquid-electrolyte case of mobile countercharge in Fig. 3b, which will be discussed below.

Galvanic cell model for the thin diffuse layer-limit for an liquid electrolyte

From the leading order approximation-procedure [13]-[15],[46],[50] we can derive a similar semi-analytical model for the thin-DL limit (ε→0) for the case of mobile countercharge. The results that we present here extend on those of ref. [14] by going from a purely electrolytic system with zero open circuit voltage (ϕ_0=0) to the general case of galvanic cell. In the thin-DL limit in the bulk of the electrolyte the cation concentration decreases linearly, and the concentrations just outside the two diffuse layers are related according to (Eq. (35) in ref. [14] ; Eq. (46.13) in ref. [35])

$$c_{\mathrm{sol}}^{\mathrm{C}} = c_{\mathrm{sol}}^{\mathrm{A}} - 2j \tag{30}$$

where 'sol' stands for a position just outside the diffuse layer, see Fig. 1. Thus, with $\int_0^1 c_{\mathrm{sol}}\,\mathrm{d}x = 1$ because of conservation of the total number of inert countercharge, we have $c_{\mathrm{sol}}^{\mathrm{A}} = 1 + j$ and $c_{\mathrm{sol}}^{\mathrm{C}} = 1 - j$. The potential difference across the bulk electrolyte (between the two points we mark 'sol') is given by (Eq. (37) in ref. [14])

$$\Delta\phi_{\mathrm{elyt}} = -\ln\left(1 - \frac{2j}{c_{\mathrm{sol}}^{\mathrm{A}}}\right) = \ln\frac{c_{\mathrm{sol}}^{\mathrm{A}}}{c_{\mathrm{sol}}^{\mathrm{C}}} = \ln\frac{1+j}{1-j}. \tag{31}$$

Eq. (31) is also given by Levine [35], his Eq. (46.15), but there rather lengthier, namely as a summation of minus twice the second term of Eq. (31) and once the third term to give $-\Delta\phi_{\mathrm{elyt}}$. With mobile countercharge, the structure of the diffuse layer is not described by Eq. (26) but according to the well-known Gouy-Chapman relation,

$$\Delta\phi_{\mathrm{s}} = 2\cdot\delta\cdot\sqrt{1\pm j}\cdot\sinh\left(\tfrac{1}{2}\Delta\phi_{\mathrm{D}}\right) \tag{32}$$

where we have included the fact that near the electrodes the bulk ion concentration (on which δ is based via the Debye length, λ_{D}) is modified due to a non-zero current. As before, the upper sign in $\pm$ refers to the anode, the lower sign to the cathode, which is related to the fact that j is defined positive when the cations run from anode to cathode. In dimensionless notation, the gFBV-equation becomes

$$\pm j = j_{\mathrm{O}}\exp\left(\tfrac{1}{2}\Delta\phi_{\mathrm{s}}\right) - k_{\mathrm{R}}c_{\mathrm{sol}}\exp\left(-\Delta\phi_{\mathrm{D}} - \tfrac{1}{2}\Delta\phi_{\mathrm{s}}\right) \tag{33}$$

to be applied on both electrodes, and combined with the closure-equation, Eq. (27).

For the GC- and H-limits, Eqs. (30)-(33) for the case of mobile countercharge in the thin-DL limit can be solved to give analytical expressions for ϕ_{cell} vs current j, given for the GC-limit by

$$\phi_{\mathrm{cell}} = \phi_0 - 4\cdot\operatorname{arctanh}(j) + \ln\frac{1 - j/j_{\mathrm{O,A}}}{1 + j/j_{\mathrm{O,C}}} \tag{35}$$

and for the H-limit by

$$\phi_{\mathrm{cell}} = \phi_0 - 4\cdot\operatorname{arctanh}(j) - 2\cdot\operatorname{arcsinh}\frac{j}{\sqrt{\beta_{\mathrm{A}}(1+j)}} - 2\cdot\operatorname{arcsinh}\frac{j}{\sqrt{\beta_{\mathrm{C}}(1-j)}} \tag{36}$$

which are mathematically equivalent to Eqs. (72) and (75) in ref. [14] except for the sign reversal of j (in ref. [14], j is defined to be positive for the transport of positive charges from cathode to anode, which is the opposite of the standard sign convention) and for the fact that k_{R} and j_{O} (thus β) can have different values at the two electrodes in Eqs. (35) and (36) above. In this way, we naturally extend the current-voltage relations of Eqs. (72) and (75) of ref. [14] (which describe an electrolytic cell) to galvanic cell operation. Eqs. (28) and (29) (for fixed countercharge) differ appreciably from Eqs. (35) and (36) (for mobile countercharge), which is in contrast to what we erroneously argued in ref. [17] (namely that they would be the same, irrespective of whether countercharge would be fixed or mobile).

The above analytical expressions show clearly how the cell voltage ϕ_{cell} departs from the open-circuit voltage, ϕ_0, due to polarization of the cell at nonzero current, which can be decomposed into a transport resistance, $4\cdot j$ or $4\cdot\operatorname{arctanh}(j)$, and two kinetic 'resistances'. When the kinetic constants, $j_{\mathrm{O,i}}$ or

β_i, are very large, the transport resistance dominates, while electrode kinetics dominates when on at least one of the electrodes $j_{O,i}$ or β_i is very small.

Fig. 3 shows calculation results for a galvanic cell with fixed countercharge (Fig. 3a) and for mobile countercharge (Fig. 3b) using the model in the thin-DL limit, where general results are shown as function of the parameter δ based on Eqs. (23)-(27) for fixed countercharge, and Eqs. (30)-(33) for mobile countercharge, as well as limiting results for the GC- and H-limit. Reaction-limited currents in the GC-limit are observed for $j=-j_{O,C}=-0.2$ and for $j=j_{O,A}=0.8$, as well as diffusion-limited currents at $j=\pm1$ for mobile countercharge (Fig. 3b). We also note an interesting difference between Fig. 3a (fixed countercharge) and Fig. 3b (mobile countercharge) that in Fig. 3b we need a much larger range of δ-values to go from close to the H-limit to close to the GC-limit (~factor of 1000) than in Fig. 3a (~factor of 100).

Another interesting effect, not mentioned previously, is the possibility of non-monotonic dependence of the cell voltage ϕ_{cell} on the parameter δ (for given current j). A clear manifestation of this effect is seen in the upper-left corner of Fig. 3b where for $\delta=1$ and $\delta=10$ for $j=-0.9$ the cell voltage ϕ_{cell} is smaller than predicted by the H-limit. This shows that the GC- and H-limits, in spite of representing the limiting behavior for $\delta\to0$ and $\delta\to\infty$ and conveniently approximating the "envelope" of possible charge-voltage relations, do not strictly bound the range of possible values for j-ϕ_{cell} when δ is in between 0 and ∞. The reason, illustrated in the insert of Fig 3b is that the double layer potentials $\Delta\phi_i$ at the two electrodes ($\Delta\phi_i=\Delta\phi_s+\Delta\phi_D$) have different dependencies on δ, and can in some cases combine to give the total cell voltage ϕ_{cell} a non-monotonic dependence on δ. In this particular case, for $j=-0.9$, the ion concentration near the anode is reduced by a factor 10 and increased at the cathode by a factor of 2, see Eq. (30). Thus the Debye length is much smaller at the cathode and thus, on increasing δ, the effect of the Stern layer becomes apparent earlier than on the anode.

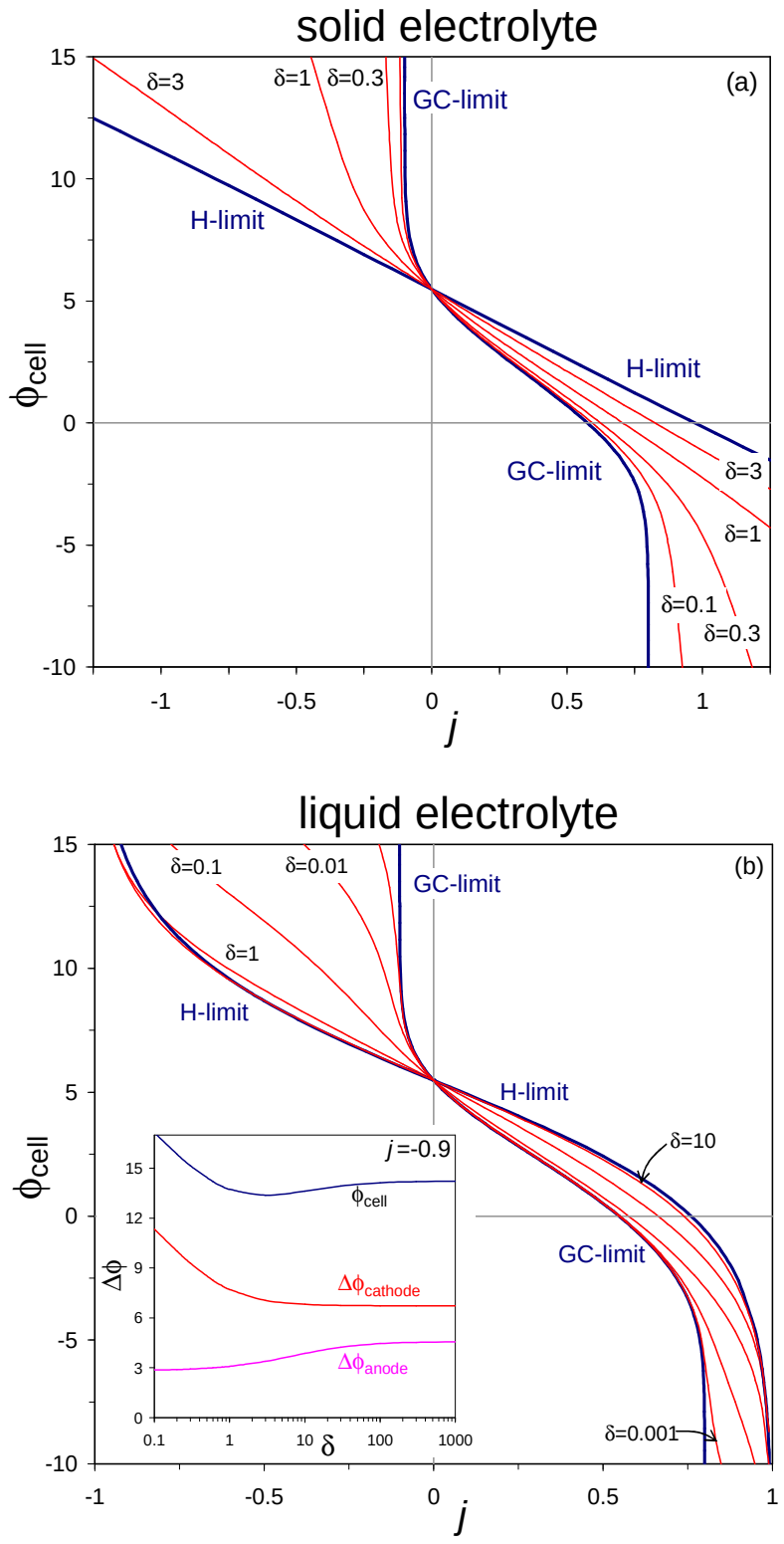

Fig. 3. Cell voltage vs. current for a galvanic cell with fixed (a) and mobile (b) countercharge, operating in all three modes identified in Fig. 1 in the thin-diffuse layer (zero-ε) limit based on Eqs. (23)-(36) ($j_{O,A}$=0.8, $j_{O,C}$=0.1, $k_{R,A}$=1, $k_{R,C}$=30). Reaction-limited current is obtained in the GC-limit when $j \to j_{O,A}$ or $j \to -j_{O,C}$, while in the H-limit the current is diffusion-limited when $j \to \pm 1$, but only for mobile countercharge. Insert in (b) shows non-monotonic dependence of ϕ_{cell} on δ.

Reaction-limited current and diffusion-limited current

The above set of equations can be used to discuss briefly two types of limiting currents that are predicted in theories of galvanic cells, which are apparent in Fig. 3. Firstly, in the GC-limit (for both materials, with fixed or mobile countercharge) a reaction-limited current is predicted in Eqs. (28) and (35) when $j \to j_{O,A}$ or $j \to -j_{O,C}$. This mathematical limit was discussed previously in refs. [13] and [14], and is due to the unphysical assumption of a zero thickness of the Stern layer, and thus the disappearance of the voltage-dependent Arrhenius term from the gFBV charge-transfer rate equation. Taking a non-zero value for δ eliminates this artificial limit, though its effect can still be seen as a steepening of the curve for ϕ_{cell} vs. j ("*V-i* curve"). Secondly, for the material with mobile countercharge, Eqs. (35) and (36) contain a term arctanh(j) which will diverge for $j \to 1$ and $j \to -1$. These are the classical diffusion-limited currents [14],[15],[54], which are predicted in the thin-DL limit for a material with mobile countercharge. Although in reality most electrochemical cells have thin diffuse layers compared to the bulk dimensions, it must be formally noted that, as discussed in refs. [14], [15] and [31], in any calculation with a non-zero value for ε (which is required for a finite-thickness membrane) the diffusion-limited current is eliminated, although it will result in a steepening of the *V-i* curve. For any finite DL thickness, with a sufficiently large voltage and/or small system, it is possible to reach the regime of "super-limiting current" in the model, where the diffuse layer expands to a non-equilibrium structure, as first described by Rubinstein and Shtilman [31] in the context of electrodialysis. In summary, our full PNP-gFBV model does not predict any true limiting currents, but only a steepening of the *V-i* curve. It is only when either of the parameters ε or δ tends to zero that true singularities in the *V-i* curve (or plateaus in the *i-V* curve) are predicted.

It is interesting to note that in more complicated situations diffusion-limited currents can also arise in a full PNP-gFBV model for non-zero ε. Our analysis assumes a single reactive ion that can react to/from its reduced state at constant chemical potential in the two electrodes. A more general situation is that the current also influences the interfacial concentration of the product species. For instance, in the case of a neutral product species which must shuttle between the electrodes as in refs. [13], [28], [29] and [30], there is an overall balance of reactive plus neutral species, and thus diffusion limitation of the neutral species can yield a limiting current for the entire cell, under some conditions, even in a full model with all length scales finite ($\delta>0$ and $\varepsilon>0$).

Analysis of energy losses during charging-discharging cycles

Analytical equations such as Eqs. (23)-(36) presented above can be very valuable to use in an analysis of energy storage and conversion in reversible galvanic cells. For example, these equations can be applied to predict the energy efficiency of redox flow cells, where parameters $j_{O,i}$ can be made a function of the chemical state of the reduced species (e.g., dependent of the time-varying hydrogen gas pressure during charging of a redox flow cell based on electrolytic hydrogen compression). For energy-efficient charging and discharging it is clearly best to stay close to the open circuit voltage ϕ_0, although this may overly constrain the desired rates of charging and discharging. Analysis on the basis of Eqs. (23)-(36) can show to what extent the cell potential ϕ_{cell} will diverge if the charging current ($j<0$ during charging) is too large, which implies large losses during energy storage and poor

efficiency of energy storage. In particular, the energy efficiency, η, defined as the work done by the cell upon discharge at current $j_{\text{discharge}} > 0$ (converting chemical to electrical energy) divided by the external work done to recharge the cell at current $j_{\text{charge}} < 0$ (converting electrical back to chemical energy), is given by $\eta = \frac{\phi_{\text{cell}}(j>0)}{\phi_{\text{cell}}(j<0)}$ when the cell voltage remains at a constant value during the charging phase, as well as during discharge.

Results and Discussion

Solid electrolyte

First we show results for the cell voltage-current characteristic of a fuel cell with immobilized countercharge. We take the example of a hydrogen concentration cell in which mobile protons in the electrolyte are electrochemically exchanged with gaseous hydrogen at the electrodes (via an assumed equilibrium of H_2 in the gas phase with adsorbed hydrogen atoms near the charge-transfer site) [16],[24]. To generate a positive cell voltage, the anode compartment hydrogen pressure $p_{\text{H2,A}}$ is larger than in the cathode compartment, $p_{\text{H2,C}}$. The calculation is based on both the complete PNP-gFBV model (using Eqs. (14)-(17)) and the model in the thin-DL limit, based on Eqs. (23)-(27). Parameter settings in the calculation for Fig. 4 are as follows. For the model in the thin-DL limit we require $p_{\text{H2,A}}$=1 bar, $k^*_{\text{A}}=k^*_{\text{C}}=10^5$ A/(m^2·bar$^{1/2}$), p^*=1 μbar, R^*_{elyt}=1 m^2/A, $f^{-1}=RT/F$=68.9 mV, and δ=1. These parameter settings translate into those required for the full dimensionless PNP-gFBV model when using the conversion formula given below Eq. (27). As long as in the full model sufficiently thick membranes are considered, i.e., for low values of ε (below ε~0.01), results are virtually identical to those of the thin-DL limit.

In Fig. 4 we show the dependence of V_{cell} on current density, i, for different cathode hydrogen pressures. The fuel cell spontaneously generates a current (galvanic discharging mode) for currents between zero and a maximum value, i_{max}, while outside this range a current is imposed, both for currents below zero (electrolytic charging), and for currents above i_{max} (super-galvanic regime). For large positive currents, the cell acts like a resistor, set by the bulk membrane resistance, but for negative currents, signs of a reaction-limited current, or diverging surface overpotential, appear with decreasing cathodic hydrogen concentration. Interestingly, we do not find strong effects of the applied cathode gas pressure, $p_{\text{H2,C}}$, when we operate the cell galvanically, but very strong differences develop when a negative current is imposed on the cell. Such experiments clearly would be very useful to provide informative and sensitive data to validate models for galvanic cell against. The strong asymmetry predicted in the curves for V_{cell} vs i around i=0 shows that overpotentials are not identical (for a given magnitude of the current) when we go from the forward (fuel cell) to the backward (electrolytic cell) mode, which is different from what follows from more conventional Butler-Volmer modeling [5].

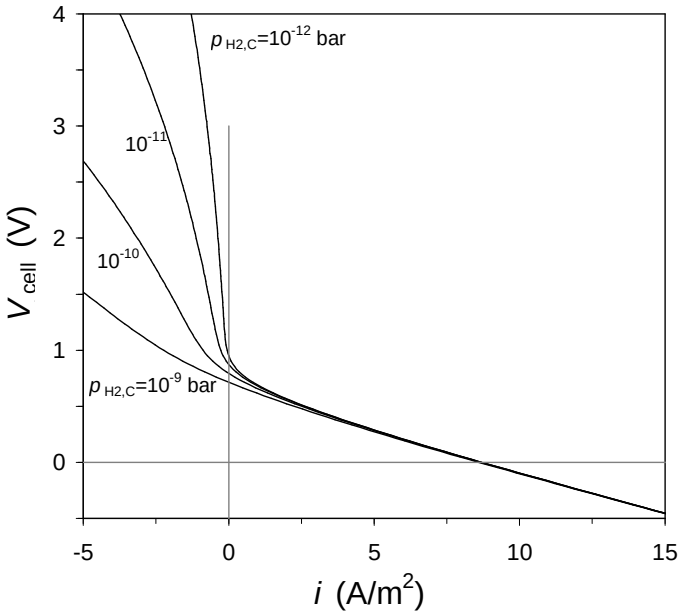

Fig. 4. Voltage-current characteristic for a hydrogen fuel cell which operates galvanically between $0<i$ (A/m^2)<7. A current is imposed upon the cell (not generated spontaneously) when V_{cell} and i have opposite signs, such as to the left of the i=0-axis (electrolytic charging), and beyond i~7 A/m^2 (super-galvanic regime). Parameter settings in main text.

Next we show in Fig. 5 profiles across the electrolyte membrane for the proton concentration, and for the electrostatic potential. From this point onward all calculation results that will be presented are based on the dimensionless complete PNP-gFBV model with non-zero values for ε. In order to illustrate the continuous potential profile across the reaction plane in the model, in all subsequent figures (except Fig. 7) we include the compact Stern layers in plots of the electrostatic potential profile extending from electrode to electrode, not only across the continuum regions with dimensionless coordinate $0<x<1$. In these graphs, coordinate x is rescaled in such a way that the continuum space in between the Stern planes (which are represented by the dashed vertical lines in the graphs) runs from position $\delta/(1+2\cdot\delta)$ to $1-\delta/(1+2\cdot\delta)$. For simplicity, we assume a permittivity ratio of unity between the electrolyte and compact Stern layer, so that the potential extrapolates linearly across the Stern layer with the limiting slope from the edge of the electrolyte.

In Fig. 5, all dimensionless concentrations c^+ and c^- are dimensional concentrations C^+ and C^- scaled to the ionic strength C_∞ (concentration of each of the ions in the uncharged membrane). Calculation results are presented for ε=0.03 (Debye length 3% of the distance between the Stern planes of each electrode), for $k_{R,A}=k_{R,C}=1$, $j_{O,A}=2$, $j_{O,C}=0.5$, with the anode located to the left end of each graph, and the cathode on the right end. The chosen values for $k_{R,i}$ and $j_{O,i}$ imply that at equilibrium (j=0) according to $\phi_0 = \ln k_{R,C} j_{O,A} k_{R,A}^{-1} j_{O,C}^{-1}$, the dimensionless open circuit voltage $\phi_0=f\cdot V_0$ is given by $\phi_0=\phi_{m,C}-\phi_{m,A}=\ln(4)=1.39$, which is in accordance with Fig. 5b (curve for j=0; ϕ_0 is the difference between the value for ϕ at the very right of the curve, $\phi_{m,C}$, minus that at the very left, $\phi_{m,A}$).

For equilibrium, Eq. (9) gives the total voltage difference over each double layer $\Delta\phi_T$ (where $\Delta\phi_T$ is a summation of the voltage difference over the diffuse part, $\Delta\phi_D$, and that over the Stern layer, $\Delta\phi_s$),

which can be written in dimensionless units as $\Delta\phi_T = \ln\left(k_R j_O^{-1}\right)$. The full calculation gives the same result, with for j=0 $\Delta\phi_T$=-ln(2) at the anode and $\Delta\phi_T$=+ln(2) at the cathode. However, this does not imply that the equilibrium structure of the double layer is the same on both electrodes, because in this case protons are expelled on one electrode and are attracted to the other, which results in a different structure of the diffuse layer, and thus a different value for the diffuse charge (which determines $\Delta\phi_s$). Indeed, on the cathode we obtain in this case a slightly higher magnitude of the diffuse layer potential $\Delta\phi_D$ (and thus a lower $\Delta\phi_s$) than on the anode.

Fig. 5a shows concentration profiles shifted up- or downward by multiples of 0.2 to increase readability (except for the curve for j=0.5, which is not modified). For positions between 0.2 and 0.8 all concentrations c^+ are very close to unity. Fig. 5b shows the corresponding dimensionless electrostatic potentials ϕ as function of position. Thin layers to the very left and right in each graph represent the Stern layer, with the Stern planes shown as dashed vertical lines in Fig. 5b. Fig. 5b shows how the cell voltage $\phi_{cell}=\phi_{m,C}-\phi_{m,A}$ is positive for a current of j=0.20 and below. As galvanic (spontaneous) operation requires both a positive j and a positive value for ϕ_{cell}, galvanic operation for the present parameter settings is only observed for $0 \le j \le 0.20$. Below j=0 we have electrolytic conditions with an imposed current which is in the opposite direction compared to the current direction for 'normal' galvanic operation, i.e., we push electrons 'in reverse' and pump hydrogen gas from the low pressure side to the high pressure side. This is the situation where excess electrical energy is stored in the form of compressed hydrogen gas, which we have called 'electrolytic charging' in Fig. 1. In contrast, the 'super-galvanic regime' requires an imposed current beyond the maximum that can be provided in galvanic operation, namely when the external resistance is zero (j_{max}~0.20). This regime is represented in Fig. 5 by the curves ranging from j=0.50 to j=2.0.

As shown in Fig. 5a we have at equilibrium (j=0) an excess of protons on the anode and a deficit on the cathode. As discussed previously [13],[14],[17] there is no theoretical constraint for the two diffuse charge densities to exactly compensate one another, i.e., there is no requirement for the total membrane charge to be zero, not even at equilibrium. The only constraint is that the total charge on all electrodes combined plus the charge in the electrolyte membrane must sum to zero so that the entire system is electrically neutral. However, there is no requirement for the electron charge and the diffuse charge on any electrode to exactly compensate one another (except in equilibrium). Instead, the difference between the two values of charge (which for thick membranes will be small) determines the field strength just outside the diffuse layer and thus the migration current into the bulk electrolyte. In Fig. 5a we observe that with increasing currents first the cathode diffuse layer becomes uncharged (just beyond j=0.5) and slightly later the same occurs for the anode diffuse layer (slightly beyond j=1.0). Beyond that point, for j=1.5 and j=2.0 in Fig. 5a, we obtain concentration profiles which are completely reversed compared to the situation below j=0.5, with now an excess of protons on the cathode, and a deficit on the anode. These diffuse layer profiles at high currents provide for the 'reverse' reduction reaction of the proton on the anode to be suppressed (which requires the proton concentration at the anode to go down) and thus the net reaction rate to go up. Vice-versa, the proton concentration is increased at the cathode to increase its reduction rate there and thus to increase the

proton conversion rate. The reversal of the sign of the diffuse charge upon changing the current from very negative to very positive is a general phenomenon and can also be found for electrolytic cells, also for the case of mobile countercharge [14][15], and even for a cell where at equilibrium the diffuse layers are uncharged.

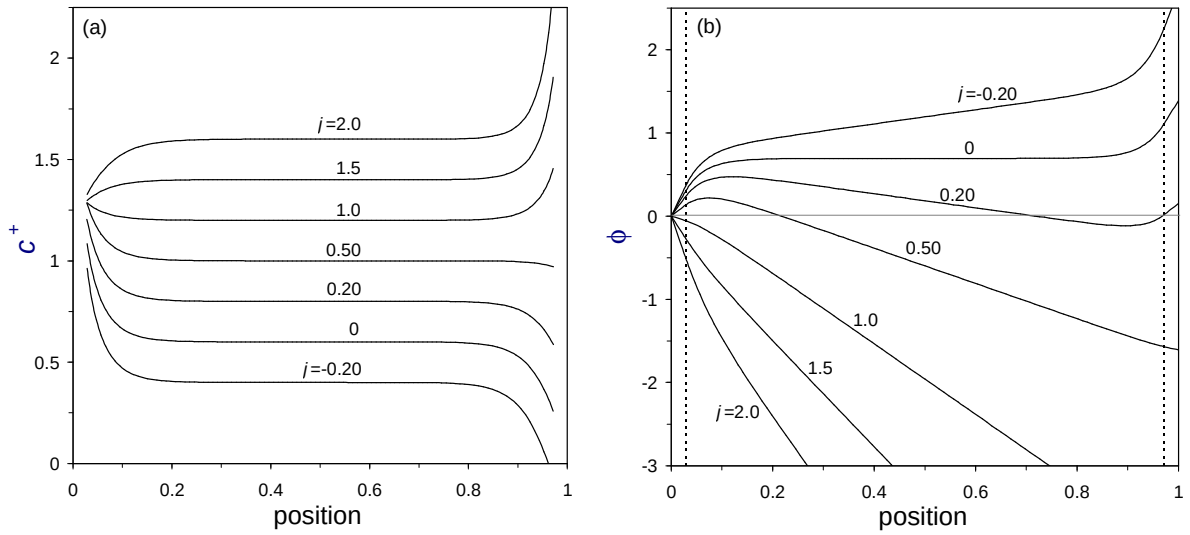

Fig. 5. Proton concentration (c^+) and electrostatic potential (ϕ) profiles for a fuel cell with fixed countercharge operated at various values of the dimensionless current j. The anode is located left and the cathode right. For currents $0 \leq j \leq 0.20$ the cell functions as a galvanic cell while outside this range a current must be imposed on the cell. Dashed lines in b) denote the Stern plane. In a) the profiles are shifted up- and downward for clarity; in the bulk the dimensionless concentration is ~1 for all conditions.

Finally we show in Fig. 6 results for j=0.1 and for galvanic conditions, i.e., $\phi_{m,C} > \phi_{m,A}$, which implies we consider situations where electrical energy is generated. We vary the values of $j_{O,A}$ and $j_{O,C}$ but by keeping their ratio constant at $j_{O,A}/j_{O,C}$=4 the open cell voltage remains at ϕ_0=1.39. By varying the values of $j_{O,i}$ we obtain the three situations as discussed in ref. [17]:

1. both $j_{O,A}$ and $j_{O,C}$ are below $k_{R,i}$ (which is unity for both electrodes) and we have the situation that on both electrodes we have a proton deficit (Case III in Fig. 2 in ref. [17]);
2. only $j_{O,A}$ is above $k_{R,i}$ and we have a proton deficit on the cathode and a proton excess on the anode (Case I in Fig. 2 in ref. [17]);
3. both $j_{O,A}$ and $j_{O,C}$ are above $k_{R,i}$ and we have a proton excess on both the anode and cathode (Case II in Fig. 2 in ref. [17]).

What Fig. 6 shows is how the structure of the polarization layer adjusts itself to the kinetic properties of the electrode reactions, such that for the steady state the current becomes constant across the system. The sign of the voltage difference across each polarization layer cannot be derived for instance from the simple fact that the cell operates as a fuel cell, generating electrical energy, unless there is a-priori information of the electrode kinetics and/or the equilibrium structure of the polarization layers (such as contained in in the value of the zero charge pressure p^* of the membrane/electrode-interface for a hydrogen fuel cell). The only constraint for spontaneous, galvanic, operation is that we cannot have a negative charge on the anode and a positive charge on the cathode because then

Kirchhoff's rule (of a zero total voltage drop around a current loop), Eq. (27), would always predict a negative cell voltage.

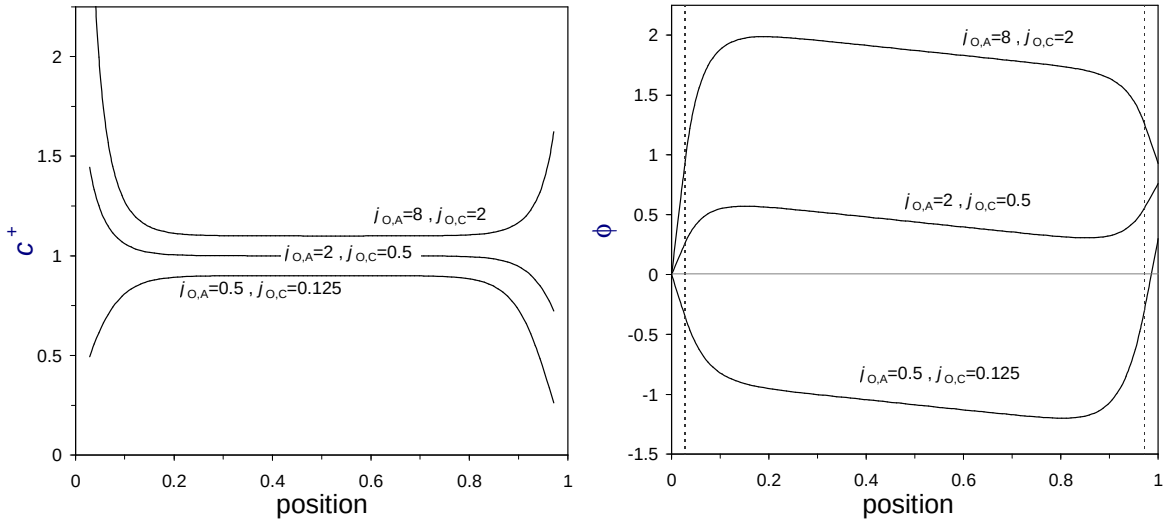

Fig. 6. Proton concentration (c^+) and electrostatic potential (ϕ) profiles for a galvanic cell with fixed countercharge (dimensionless current j=0.1, ε=0.03, $k_{R,A}$=$k_{R,C}$=1). In all cases the open cell voltage is the same, namely ϕ_0=ln($j_{O,A}$/$j_{O,C}$)~1.39.

Liquid electrolyte

The second set of calculations is based on the case that both ions are mobile, not only the reactive cation, but the inert anion as well.

Liquid electrolyte – electrolytic cell

First we discuss results of a calculation in which k_R and j_O are given the same values on both electrodes, as in refs. [14] and [15], see Fig. 7. This implies that there are no conditions that the cell operates spontaneously, but instead current can only be forced through the cell, which effectively is always in the "electrolytic charging mode" where external electrical energy is converted into chemical energy (which is then also equivalent to the super-galvanic regime). This calculation will give the same results if the current is reversed. Because we take different values for k_R and j_O the electrode is charged even at equilibrium, i.e., without imposing a current. For the parameters we choose (k_R=2, j_O=1) we have an excess of inert anions on both electrodes and both electrodes have a negative diffuse charge. Because the total anion number is fixed, the increase in anion concentration at the electrodes implies that in the bulk its concentration is decreased compared to the situation that the membrane is uncharged. For the reactive cation there is no such number balance, and its total concentration in the membrane will be below the total number in the uncharged situation, because in bulk its concentration must be equal to that of the anion (thus, lower than in the uncharged membrane) and in the diffuse layers the cation is also depleted.

In Fig. 7 we show both the cat- and anion concentration profiles for the Gouy-Chapman (GC) limit of the gFBV equation where δ=0 (Fig. 7a,b), and the general case where we use a nonzero value for δ, namely δ=1 (Fig. 7c,d). As discussed before, in the GC-limit a maximum current can be reached (the

reaction-limited current) because the GC-limit assumes that the Stern potential difference $\Delta\phi_s$ is zero. Thus, Eq. (8) can be rearranged to give

$$c_{O,A} = \frac{j_{O,A} - j}{k_{R,A}} \quad , \quad c_{O,C} = \frac{j_{O,C} + j}{k_{R,C}} \tag{34}$$

which predicts negative concentrations for imposed currents $j \geq j_{O,A}$ or $j \leq -j_{O,C}$. This shows that formally the GC-limit of the gFBV equation is an unphysical approximation, and we should ideally always use a value of $\delta>0$. Eq. (34) implies that for the parameter settings of Fig. 7, the reaction-limited currents in the GC-limit are $j_{\text{reaction-limited}}=\pm j_{O,i}=\pm 1$. Indeed, when the current j approaches unity, Fig. 7a,b shows clear signs of reaction-limitation near the anode, where the cation concentration approaches zero. Another aspect of Fig. 7a,b is that in the thin-DL ($\varepsilon=0$) limit, $j=\pm 1$ is also the diffusion-limited current. Though in the present calculation a finite ratio for Debye length over membrane thickness is used ($\varepsilon=\lambda_D/L=0.05$), this diffusion limitation will also affect the ion concentration and potential profiles, leading to an expansion of the cathodic diffuse layer (extended "space charge" region) characterized by a nearly complete expulsion of anions, the properties of which can be analyzed on the basis of asymptotic analysis [14],[15],[54]. According to this analysis, when j reaches beyond $1-(2\varepsilon)^{2/3}$ an expansion of the cathodic diffuse layer is expected with width of order $O(\varepsilon^{2/3})$ extending with further increasing currents [14],[31],[50]. These effects near the cathode are clearly observed in Fig. 7a,b. In particular, the double layer expands to a width of roughly $0.15 \approx \varepsilon^{2/3}$ at the cathode for $j = 0.8 \approx 1-(2\varepsilon)^{2/3}$, and then expands further at j=0.9 with near-total depletion of the anions propagating further into the bulk. A consequence of the simultaneous onset of both limitations is that the total charge in the electrolyte becomes significantly negative: at an imposed current of j=0.9, large enough to feel strong effects of both limiting currents, the total cation concentration integrated across the membrane is only 40% of its value at j=0. Meanwhile, the total anion number is fixed, and its distribution becomes highly unbalanced, with a huge increase in concentration near the anode, due to the expulsion of anions from the growing space-charge layer on the cathode, where the anion concentration drops to a few ppm already at j=0.9.

The reaction-limited current is avoided for any non-zero value of δ. Indeed, if we choose $\delta=1$ we are easily able to solve the model numerically far beyond j=1 and can thus present in Figs. 7c,d results up to j=1.5. Furthermore, even at that current the total cation number (integrated over the full membrane) does not deviate significantly from the value of the uncharged membrane. The anion density profile is also much less peaked near the anode and decreases much more gradually from anode to cathode. At the cathode its value is low but even at j=1.5 it is still as large as ~0.1% of the value in the uncharged state (instead of ppm's which was already reached at j=0.9 in the case of $\delta=0$).

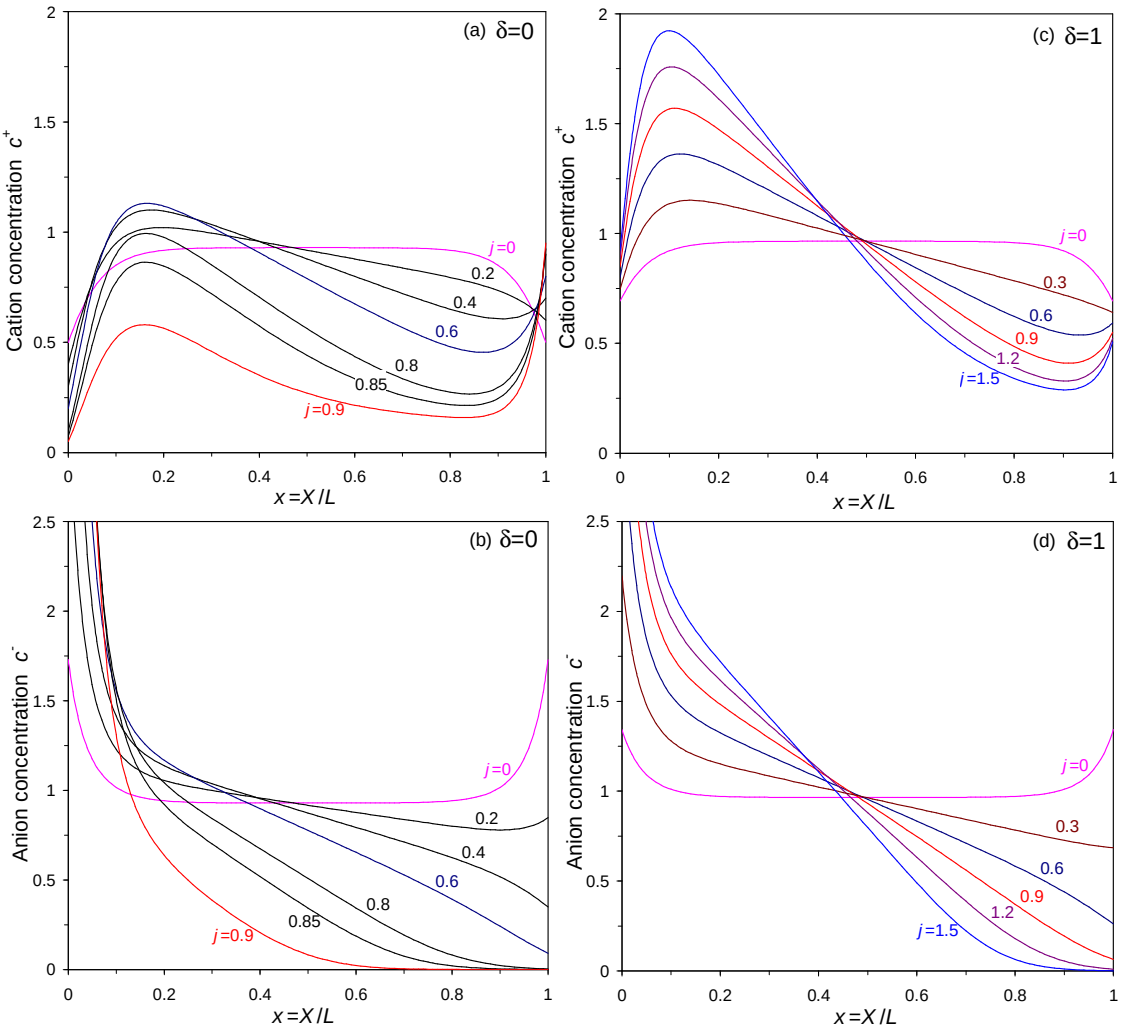

Fig. 7. Ion concentration profiles in a liquid electrolytic cell with reactive cations and all ions mobile, at various values of the current j and for $\delta=\lambda_S/\lambda_D$ either zero or unity (on both electrodes: $j_{O,i}=1$, $k_{R,i}=2$, $\varepsilon=\lambda_D/L=0.05$) as function of $x=X/L$. Anode located left, cathode right.

Liquid electrolyte – galvanic cell

Next we will discuss the situation that we have unequal values for $k_{R,i}$ and $j_{O,i}$ on the two electrodes (namely, $k_{R,A}=1$, $k_{R,C}=1$, $j_{O,A}=10$, and $j_{O,C}=1$). As a result the cell will operate galvanically in a certain range of currents and voltages, namely in between $0\leq\phi_{cell}\leq\ln(10)$. These calculations move beyond previous work (refs. [14] and [15]) where equal values for $k_{R,i}$ and $j_{O,i}$ on both electrodes were used.

In Fig. 8 we first show results for a zero current, $j=0$, which already presents interesting behavior, showing apparent interactions between the double layers, even though they do not overlap. Because at the cathode (right-hand side in the graph) $k_{R,C}$ and $j_{O,C}$ are equal to one another, one would naively expect that there all concentration profiles, as well as the potential profile, remain flat (no diffuse charge). However, in Fig. 8 we unexpectedly do observe the development of a diffuse layer. The explanation of this effect is as follows, and relates to the fact that the membrane is relatively thin. However, the effect is not due to a double layer overlap between the anode and cathode diffuse layers, but instead is due to a modification of the bulk ion concentration due to the very pronounced diffuse layer that forms on the other electrode, the anode. The diffuse layer formation on the anode in

the equilibrium state is due to the large difference between $k_{R,A}$ and $j_{O,A}$. Because a very negative diffuse layer potential difference develops, anions are expelled from the interface region into the bulk of the membrane, leading to an anion bulk concentration increase. In order to maintain bulk quasi-neutrality, this requires additional cations, which are synthesized from an oxidation at the anode until the cation bulk concentration equals that of the anions. This increase in bulk cation concentration has an effect on the equilibrium diffuse layer structure on the cathode, and by combining $c_O=c_\infty^*\cdot\exp(-\phi_D)$ with Eq. (9) we obtain the equation $\Delta\phi_T=\ln(j_O/(k_R\cdot c_\infty^*))$ which we can use to rationalize that for the cathode (where $j_O=k_R$) this increase of c_∞^* will result in a potential drop near the cathode, i.e., $\Delta\phi_{T,C}<0$, and therefore the development of a negative excess diffuse charge. This effect is generally to be expected whenever one electrode "X" is able to modify the bulk solution concentration to some extent and in this way will affect other electrodes, resulting in a modification of the diffuse layer structure there, even for zero current, without double layer overlap, and when the other electrode was uncharged in the absence of the electrode X.

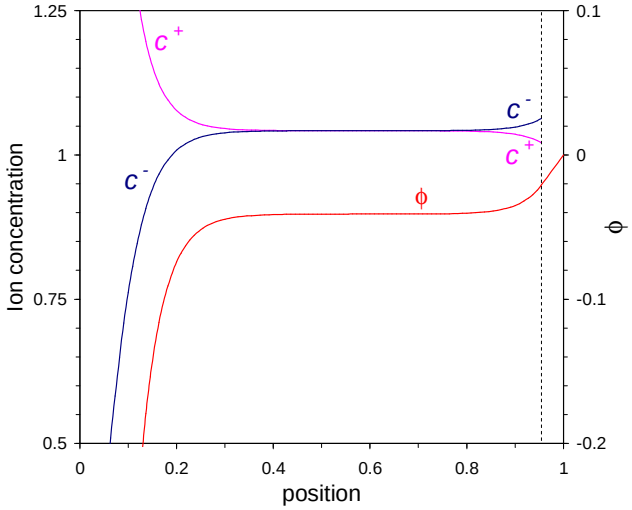

Fig. 8. Equilibrium ion concentration and potential profiles in a liquid galvanic cell with reactive cations and all ions mobile (open-circuit condition, thus current j=0, δ=1, $j_{O,A}$=10, $j_{O,C}$=1, $k_{R,A}=k_{R,C}$=1, ε=0.05). Anode located left, cathode right.

In Fig. 9 we show results for the parameter settings of Fig. 8 for currents above and below zero, in all three ranges as shown in Fig. 1. Fig. 9a shows both an- and cation density profiles, and Fig. 9b the electrostatic potential profile. In Fig. 9a ion concentrations are shifted up- and downward by steps of Δc=0.2, to increase clarity of presentation. Without the vertical shift in the concentration profiles, in all cases c^+ is ~1 at the cathode. Fig. 9a shows that in the bulk of the membrane the anion and cation concentrations are about equal, up to the upper boundary of galvanic operation, around j=0.5. Because of the pronounced voltage difference over the anode polarization layer, its structure is relatively unperturbed by the applied current. On the other hand, on the cathode the net diffuse charge switches sign when going from negative to positive current. The potential profiles in Fig. 9b show again how on the anode the diffuse layer voltage difference is not greatly influenced by current, whereas on the cathode it changes sign around j=0. The insert shows the cell voltage as function of

current and shows that the regime for galvanic operation is in between $0<j<0.45$, with imposed currents outside this range.

A final comment can be made based on the results shown in Fig. 9, namely on the use of the terminology 'positive' and 'negative' electrodes often found in the literature. When polarization layer effects are considered, care must be taken to use such terms only when it is clear if one refers to the cell potential, the excess charge in the diffuse layer, or to the electronic charge on the electrode. To show for instance that the sign of the electronic charge and of the cell potential are not directly related, consider for instance that in Fig. 9 for j=0.1 on both electrodes there is an excess positive charge of the ions in the diffuse layers, while the cathode is at a positive potential with respect to the anode (cell potential $\phi_{cell}>0$). At j=0.7 the signs of the diffuse layer charge on the electrodes are the same as for j=0.1, but the sign of the cell potential has reversed.

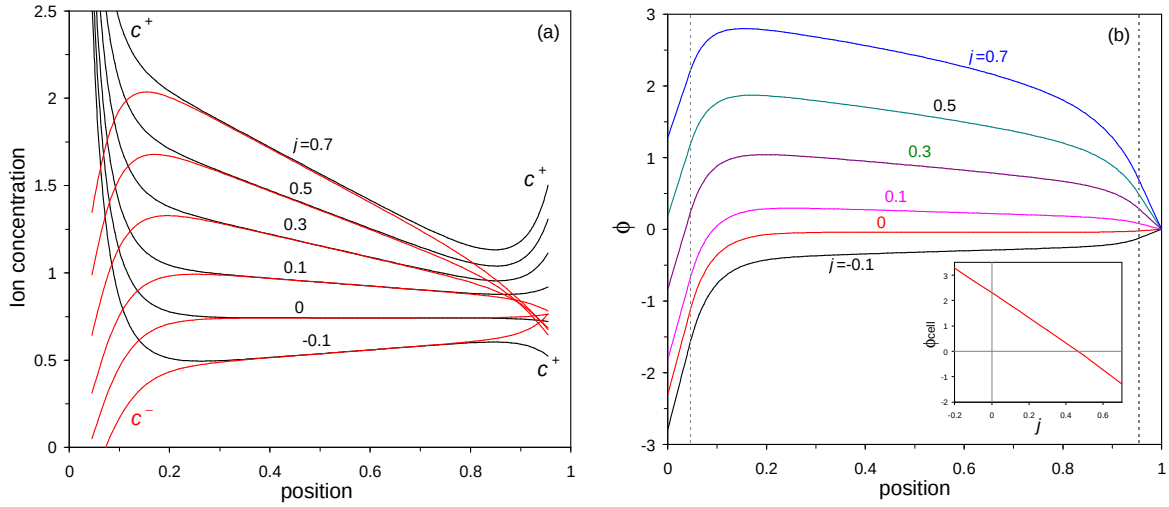

Fig. 9. Ion concentration and potential profiles in a liquid galvanic cell with reactive cations and all ions mobile (parameter settings as in Fig. 8 except for current j). Concentrations are shifted vertically in a). Dashed vertical lines in b) denote the Stern planes. The insert picture presents the cell voltage as function of current.

Conclusions

We have developed a general mathematical framework to describe the steady response of galvanic cells to the full range of spontaneous and imposed currents, which yields simple analytical results in the asymptotic limit of thin double layers, as well as a convenient system for numerical simulation. These results should be widely applicable to fit and interpret experimental current-voltage measurements in galvanic cells, such as fuel cells and batteries, and to test different theoretical assumptions. In particular, for thin double layers, by considering both the Helmholtz limit (of zero diffuse-layer thickness) as well as the Gouy-Chapman limit (of zero Stern-layer thickness), we have derived two pairs of simple, analytical charge-voltage relations for galvanic cells, which approximately bound the possible behavior of the model in the thin-double layer regime. One pair of charge-voltage relations (28)-(29) describes solid electrolytes with fixed counter-charge, and the other (35)-(36) describes binary liquid electrolytes with mobile ions. As shown in Fig 3, these analytical formulae, and numerical results for intermediate values of the ratio δ of the Stern and Debye lengths, predict a wide range of behavior in the charge-voltage relation, which can be applied to experimental measurements.

Additionally, these simple theoretical predictions can be used to analyze the efficiency of energy storage in reversible galvanic cells and can be applied to place limits of the acceptable rates of charging and discharging to control energy losses.

In our model, the generalized Frumkin-Butler-Volmer (gFBV) equation is combined with the Stern model for continuity of the electric displacement field across the reaction plane, to give the required boundary conditions for the Poisson-Nernst-Planck (PNP) theory for mass transfer of charged species. The PNP equations describe the potential and ion profiles in the electrolyte bulk and diffuse part of the polarization layer alike, without making an artificial distinction between bulk and diffuse layer, and without implicitly assuming local or overall electroneutrality. Indeed, though in an electrochemical cell, the membrane electrolyte phase plus the electrodes will be overall electroneutral, the electrolyte generally has a non-zero overall charge. In the generalized gFBV-PNP model with a finite electrolyte membrane thickness and for the case of a single reactive ion that reacts to/from a species at fixed potential, the unphysical concepts of a diffusion-limiting current (which is only predicted for the case of mobile countercharge) and reaction-limited current (for both mobile and fixed countercharge) are avoided if one assumes a non-zero Stern-layer thickness ($\delta > 0$) and a non-zero Debye-length ($\varepsilon > 0$), respectively. Instead, the model allows any cell voltage or current to be achieved when realistic physical length scales are used.

Relevant experimental information can be obtained of fuel cell operation by imposing an electrical current upon a galvanic cell, either by reversing the current direction, or by operation in the super-galvanic regime where the imposed current is larger than the spontaneous galvanic cell current in the limit of a shorted electrical circuit. Especially at high magnitudes of the imposed currents, the experimental data that are obtained can be used as a sensitive test to derive microscopic information and to distinguish between different theoretical models, as illustrated in Fig. 3. A proper model for galvanic cells should be able to describe data equally well when the cell is run in a forward mode (galvanic operation, i.e., production of electrical energy, and in the super-galvanic regime) and when it is run in the backward mode (electrolytic charging, i.e., conversion of electrical into chemical energy) using a single set of parameter settings. In general, we conclude that experiments on galvanic cells should explore the full range of imposed currents for a more stringent test of theoretical models.

References

[1] J.A. Trainham, J. Newman, *Electrochimica Acta* 26 (1981) 455.

[2] M. Bartolozzi, *J. Power Sources* 27 (1989) 219.

[3] C. Ponce de León, A. Frías-Ferrer, J. González-García, D.A. Szánto, F.C. Walsh, *J. Power Sources* 160 (2006) 716.

[4] K. Fatih, D.P. Wilkinson, F. Moraw , A. Ilicic, F. Girard, *Electrochem. Solid State Lett.* 11 (2008) B11.

[5] M. Ni, M.K.H. Leung, D.Y.C. Leung, *J. Power Sources* 163 (2006) 460.

[6] O.A. Marina, L.R. Pederson, M.C. Williams, G.W. Coffey, K.D. Meinhardt, C.D. Nguyen, E.C. Thomsen, *J. Electrochem. Soc.* 154 (2007) B452.

[7] M. Ni, M.K.H. Leung, D.Y.C. Leung, *J. Power Sources* 177 (2008) 369.

[8] J. Udagawa, P. Aguiar, N.P. Brandon, *J. Power Sources* 180 (2008) 354.
[9] A. Hauch, S.D. Ebbesen, S.H. Jensen, M. Mogensen, *J. Mater. Chem.* 18 (2008) 2331.
[10] D. Linden, *Handbook of Batteries* (McGraw-Hill, New York, 1995).
[11] D. Danilov, P.H.L. Notten, *Electrochimica Acta* 53 (2008) 5569.
[12] G. Singh, G. Ceder, M. Z. Bazant, *Electrochimica Acta* 53 (2008) 7599.
[13] A. Bonnefont, F. Argoul, M.Z. Bazant, *J. Electroanal. Chem.* 500 (2001) 52.
[14] M.Z. Bazant, K.T. Chu, B.J. Bayly, *SIAM J. Appl. Math*. 65 (2005) 1463.
[15] K.T. Chu, M.Z. Bazant, *SIAM J. Appl. Math*. 65 (2005) 1485.
[16] A.A. Franco, P. Schott, C. Jallut, B. Maschke, *Fuel cells* 7 (2007) 99.
[17] P.M. Biesheuvel, A.A. Franco, M.Z. Bazant, *J. Electrochem. Soc.* 156 (2009) B225.
[18] D.M. Bernardi, M.W. Verbrugge, *J. Electrochem. Soc.* 139 (1992) 2477.
[19] R.F. Mann, J.C. Amphlett, M.A.I. Hooper, H.M. Jensen, B.A. Peppley, P.R. Roberge, *J. Power Sources* 86 (2000) 173.
[20] G. Murgia, L.Pisani, M. Valentini, B. D'Aguanno, *J. Electrochem. Soc.* 149 (2002) A31.
[21] F. Jaouen, G. Lindbergh, G. Sundholm, *J. Electrochem. Soc.* 149 (2002) A437.
[22] R. O'Hayre, S.-W. Cha, W. Colella, F.B. Prinz, *Fuel Cell Fundamentals*, Wiley (2006).
[23] J.X. Wang, T.E. Springer, R.R. Adzic, *J. Electrochem. Soc.* 153 (2006) A1732.
[24] W.G. Bessler, S. Gewies, M. Vogler, *Electrochim. Acta* 53 (2007) 1782.
[25] K.C. Neyerlin, W. Gu, J. Jorne, H.A. Gasteiger, *J. Electrochem. Soc.* 154 (2007) B631.
[26] L. Pisani, G. Murgia, *J. Electrochem. Soc.* 154 (2007) B793.
[27] S. Kakaç, A. Pramauanjaroenkij, X.Y. Zhou, *Int. J. Hydrogen Energy* 32 (2007) 761.
[28] W.D. Murphy, J.A. Manzanares, S. Mafé, H. Reiss, *J. Phys. Chem.* 96 (1992) 9983.
[29] A.A. Moya, J. Castilla, J. Horno, *J. Phys. Chem.* 99 (1995) 1292.
[30] D.C. Prieve, *Colloids Surfaces A* 250 (2004) 67.
[31] I. Rubinstein, I. Shtilman, *J. Chem. Soc. Faraday Trans. II* 75 (1979) 231.
[32] C.P. Smith, H.S. White, *Anal. Chem.* 65 (1993) 3343.
[33] A. Frumkin, *Z. Physik. Chem.* 164A (1933) 121.
[34] M.J. Weaver, F.C. Anson, *J. Electroanal. Chem.* 65 (1975) 711.
[35] V.G. Levich, *Physicochemical Hydrodynamics,* Prentice-Hall (1962).
[36] R. Parsons, *Adv. Electrochem. Electrochem. Eng.* 1 (1961) 1.
[37] R.P. Buck, *Electroanal. Chem.* 46 (1973) 1.
[38] E.M. Itskovich, A.A. Kornyshev, M.A. Vorotyntsev, *Physica Status Solidi A* 39 (1977) 229.
[39] R. He, S. Chen, F. Yang, B. Wu, *J. Phys. Chem. B* 110 (2006) 3262.
[40] I. Streeter, R.G. Compton, *J. Phys. Chem. C.* 112 (2008) 13716.
[41] A.J. Bard, L.R. Faulkner, *Electrochemical methods*, Wiley (2001).
[42] J.S. Newman, *Electrochemical systems*, Prentice-Hall (1973).
[43] G. Prentice, *Electrochemical engineering principles*, Prentice-Hall (1991).
[44] G. Horvai, *Electroanalysis* 3 (1991) 673.
[45] M. Senda, *Electrochimica Acta* 40 (1995) 2993.
[46] M. Z. Bazant, K. Thornton, A. Ajdari, *Phys. Rev. E* 70 (2004) 021506.

[47] L.H. Olesen, H. Bruus, A. Ajdari, *Phys. Rev. E* 73 (2006) 056313.
[48] L. Gierst, *Trans. Symp. Electrode Processes* (E. Yeager, Ed.), Wiley (1959) 109.
[49] P. Delahay, *Double layer and electrode kinetics*, Wiley (1965).
[50] B. Zaltzman, I. Rubinstein, *J. Fluid Mech.* 579 (2007) 173.
[51] H. Matsuda, P. Delahay, *J. Phys. Chem.* 64 (1960) 332.
[52] T. Erdey-Grúz, *Kinetics of electrode processes,* Wiley (1972).
[53] A.A. Kornyshev, M.A. Vorotyntsev, *Electrochimica Acta* 26 (1981) 303.
[54] W. H. Smyrl, J. Newman, *Trans. Faraday Soc.* 63 (1967) 207.